Bioactive Materials 54 (2025) 901–915

Contents lists available at ScienceDirect

Bioactive Materials

journal homepage: www.keaipublishing.com/en/journals/bioactive-materials

Mesenchymal stem cell-laden double-network hydrogel nerve guidance conduits for peripheral nerve injury repair

Junghyun Kim, Junggeon Park, Seungjun Lee, Chiseon Ryu, Jongdarm Yi, Goeun Choe, Changhan Jo, Jae Young Lee *

School of Materials Science and Engineering, Gwangju Institute of Science and Technology (GIST), Gwangju, 61005, Republic of Korea

ARTICLE INFO

Keywords:
Hydrogel
Double network
Nerve guidance conduit
Peripheral nerve regeneration
Human umbilical cord mesenchymal stem cells

ABSTRACT

To enhance the repair of peripheral nerve injuries (PNIs), various nerve guidance conduits (NGCs) have been developed by integrating topological, biochemical, and cellular cues. Hydrogel-based NGCs are particularly promising owing to their unique tissue-mimicking characteristics, such as high water content, softness, and porosity. However, their weak mechanical strength and insufficient biological activity limits their application. Therefore, in this study, we aimed to develop NGCs by encapsulating human umbilical cord-derived mesenchymal stem cells (ucMSCs) in double-network (DN) hydrogel conduits for improved peripheral nerve regeneration. A DN hydrogel, fabricated via sequential photo- and ionic-crosslinking of 15 % gelatin methacrylate and 1 % alginate, exhibited excellent rheological and mechanical properties, including fatigue resistance, suture retention, and kink resistance. In a rat sciatic defect model, ucMSC-encapsulated DN NGCs demonstrated significantly improved functional and structural recovery compared to medical silicone and non-cellular hydrogel NGCs. Quantitative assessments revealed that the MSC-laden NGC group exhibited superior functional recovery, as indicated by footprint analysis, electromyography, thermal withdrawal latency, and muscle weight restoration. Moreover, histological analysis and transmission electron microscopy confirmed significantly enhanced axonal regeneration and myelination in the MSC-laden NGC group (axon diameter and myelin thickness). Overall, our results indicate that the MSC-laden hydrogel NGCs can serve as a novel platform to treat PNIs and function as effective stem cell delivery scaffolds for the regeneration of various tissues, such as the skin, tendons, and muscles.

1. Introduction

Peripheral nerve injuries (PNIs), commonly caused by trauma and disease, typically lead to numbness, muscle atrophy, and pain[1–3]. Autograft implantation is currently the gold standard treatment for severely injured peripheral nerve tissues; however, its use is limited by various issues, including the lack of appropriate donor tissues, donor site morbidity, and insufficient efficacy [4,5]. Consequently, nerve guidance conduits (NGCs) have been developed as alternatives for PNI treatment. NGCs provide physical support and guide axonal regeneration while preventing myofibroblast infiltration and scar formation [6,7]. Although several NGCs fabricated using synthetic or natural polymers have been approved by the US Food and Drug Administration for clinical application, their efficiency remains low. Therefore, extensive studies have focused on developing new functional NGCs that can deliver various biophysical and biochemical cues (e.g., mechanical properties, electrical stimuli, growth factors, and antioxidants) to enhance nerve regeneration [8,9].

Hydrogels have emerged as potential NGC materials because of their biocompatibility, porosity, high hydration, flexibility, and tissue-like softness [10,11]. However, their low mechanical strength often causes irreversible structural deformation and difficulties in handling and suturing. Unlike the central nervous system, which is shielded from external impacts by the skull and vertebral column, peripheral nerves which are often located in highly mobile areas of the body (e.g., joints) are not shielded by the bone and are susceptible to external impact and deformation [12,13]. Therefore, novel NGCs with sufficient strength to withstand external forces and stably protect the regenerating nerves during the healing process are required for efficient treatment. Several efforts have been made to improve the mechanical strength of hydrogels

Peer review under the responsibility of editorial board of Bioactive Materials.
* Corresponding author.
E-mail address: jaeyounglee@gist.ac.kr (J.Y. Lee).

https://doi.org/10.1016/j.bioactmat.2025.08.018
Received 8 October 2024; Received in revised form 11 June 2025; Accepted 16 August 2025
Available online 19 September 2025

for NGC applications, including the development of composites with reinforcing nanomaterials and double-network (DN) hydrogels [14,15]. For example, we recently demonstrated that DN hydrogels composed of gamma-ray crosslinked gelatin and ionically crosslinked alginate exhibit excellent mechanical properties suitable for NGC applications and effective peripheral nerve regeneration in a rat defect model [16]. DN hydrogels consist of interpenetrating cross-linked networks of two distinct polymers. Compared to single-network (SN) hydrogels, DN hydrogels exhibit enhanced mechanical properties because of the strong network entanglement of rigid and soft polymers and unique stress relaxation mechanisms [15].

Concurrently, recent advances in bioactive NGCs, including drug- and cell-laden platforms, have demonstrated promising results in enhancing peripheral nerve regeneration. For instance, FK506-loaded immunohydrogels were developed to modulate the inflammatory microenvironments in injured peripheral nerves and enhance myelin reconstruction [17]. In another study, adipose-derived stem cell-seeded on conductive, topographically aligned scaffolds were demonstrated to activate the PI3K-Akt pathway and promote neurotrophic cell reprogramming and peripheral nerve regeneration [18]. In particular, mesenchymal stem cells (MSCs) have been extensively studied for tissue engineering purposes, including nerve regeneration, because of their unique paracrine, immunomodulatory, and proangiogenic effects [19]. MSCs produces multiple trophic factors, exosomes, and microvesicles that can improve nerve regeneration [20–24]. Several studies have investigated the use of MSCs for the treatment of PNIs, demonstrating their potential in promoting nerve regeneration. For example, Siemionow et al. injected human MSCs (hMSCs) into the lumen of a human epineural nerve conduit, which was subsequently implanted into nude rats with sciatic nerve defects [25]. However, they observed no substantial improvements in gastrocnemius muscle regeneration and axonal density in the hMSC-injected group compared to those in the saline-injected group. Direct injection of MSCs into the NGC lumen led to poor cell stability and retention, resulting in insufficient regenerative efficacy [26]. Therefore, functional biomaterials that can effectively deliver and stably support MSCs at nerve defect sites are highly required for robust and effective nerve regeneration.

In this study, we developed a DN hydrogel composed of gelatin methacrylate (GelMA) and alginate, which synergistically combines the biocompatibility and cell-interactive properties of GelMA with the structural reinforcement from ionically crosslinked alginate. GelMA is a widely used derivative of natural gelatin that contains integrin-binding motifs (e.g., RGD sequences) supporting cell attachment, viability, and paracrine activity, while its crosslinking density can be finely tuned via photopolymerization to adjust mechanical stiffness. Alginate, a naturally derived polysaccharide, can enhance the mechanical stability and viscoelasticity of the hydrogel through ionic crosslinking with divalent cations. This DN hydrogel can provide a robust, cell-permissive matrix that supports MSC encapsulation and growth for peripheral nerve regeneration. Specifically, we developed human umbilical cord-derived MSC (ucMSC)-laden DN hydrogel NGCs via sequential photo- and ionic-crosslinking of GelMA and alginate composite hydrogels. DN hydrogel NGCs were expected to show excellent mechanical strength, long-term stability, and durability, which are desirable for suitable surgical operations, long-term mechanical protection of regenerating nerves, and prolonged support of encapsulated MSCs to produce biologically active substances. To the best of our knowledge, this is the first study to perform direct encapsulation of therapeutic cells, such as MSCs, within DN hydrogel NGCs and evaluate their efficacy in peripheral nerve regeneration. Additionally, the material properties of DN hydrogels were characterized, and the therapeutic efficacy of ucMSC-laden DN NGCs was assessed using a rat sciatic nerve defect model (Fig. 1).

2. Materials and methods

2.1. Materials

Gelatin from porcine skin (type A), alginic acid sodium salt, methacrylic anhydride, nerve growth factor (NGF) 2.5S from the murine submaxillary gland, formalin solution (10 %), poly-L-lysine solution, NaCl, $CaCl_2$, and Triton X-100 were purchased from Sigma-Aldrich (St. Louis, MO, USA). Bovine serum albumin was purchased from Bovogen

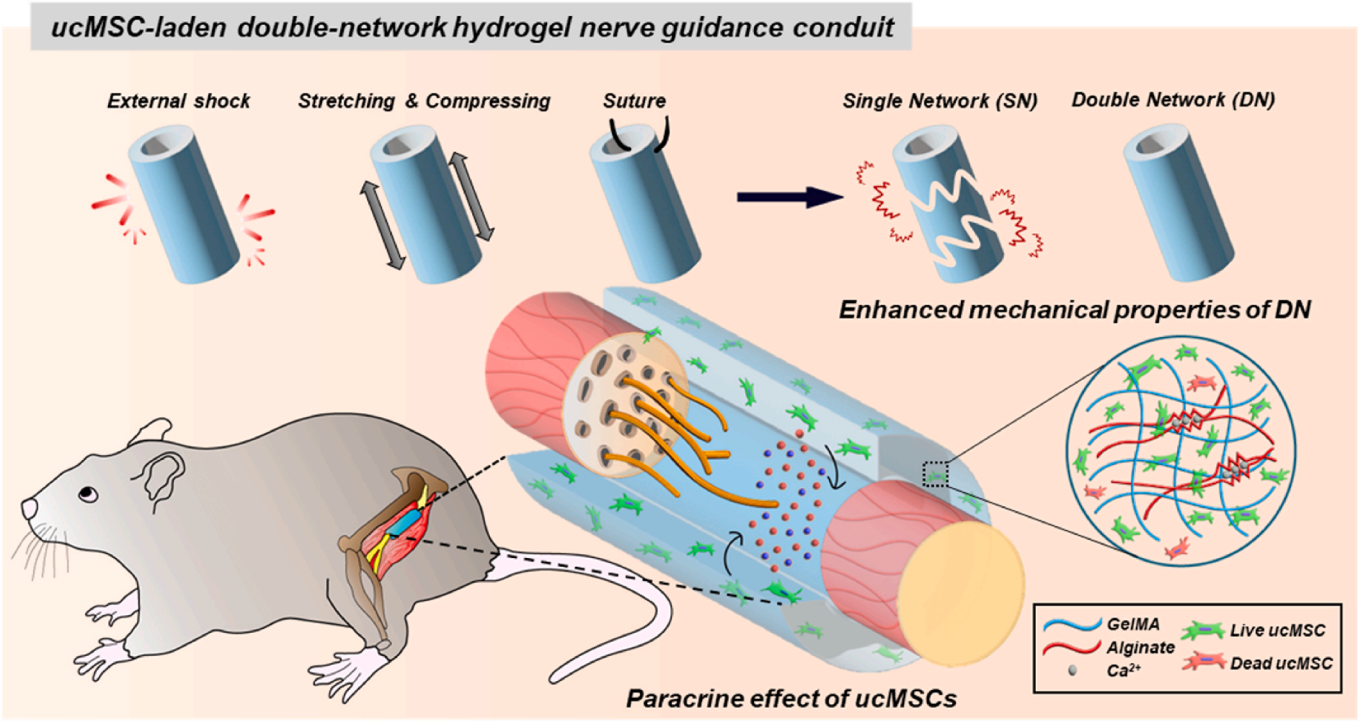

Fig. 1. Schematic illustration of umbilical cord-derived mesenchymal stem cell (ucMSC)-laden double-network (DN) hydrogel nerve guidance conduits (NGCs). ucMSC-laden DN hydrogel NGCs exhibit beneficial mechanical properties (e.g., resistance to external shock, stretching, and compression, and improved suture retention) and therapeutic activity (e.g., paracrine effects of encapsulated ucMSCs).

Biologicals (Keilor, Australia). Human ucMSCs were purchased from PromoCell (Heidelberg, Germany). Tissue culture plates (TCPs) were purchased from Thermo Fisher Scientific (Waltham, MA, USA). RAW 264.7 macrophages were purchased from the Korean Cell Line Bank (Seoul, Republic of Korea). Dulbecco's modified Eagle's medium (DMEM), neurobasal medium, fetal bovine serum (FBS), horse serum, B-27 supplement, GlutaMAX Supplement, MEM alpha, and human umbilical vein endothelial cells (HUVECs) were purchased from Gibco (Rockville, MD, USA). Lithium phenyl-2,4,6-trimethylbenzoylphosphinate was purchased from SNVia (Busan, Republic of Korea). Dulbecco's phosphate-buffered saline (DPBS), trypsin/ethylenediaminetetraacetic acid (EDTA) (0.05 %), and antibiotic–antimycotic solutions were purchased from WELGENE (Kyoungsan, Republic of Korea). An endothelial cell medium (ECM) was purchased from ScienCell (Carlsbad, CA, USA). Additionally, 4′,6-diamidino-2-phenylindole (DAPI), ethidium homodimer-1 (EthD-1), and calcein AM were purchased from Invitrogen (Carlsbad, CA, USA). Eosin Y, hematoxylin solution, and Masson's trichrome staining kits were purchased from BBC Biochemicals (Mount Vernon, WA, USA). Xylene and ethanol were purchased from Duksan Chemical (Ansan, Republic of Korea).

2.2. Fabrication of DN hydrogels

2.2.1. Synthesis and characterization of GelMA

GelMA was synthesized as previously described [10]. Briefly, 10 g of gelatin was completely dissolved in 100 mL DPBS at 37 °C. Subsequently, 8 mL of methacrylic anhydride was added dropwise to the gelatin solution at a concentration of 0.8 mL per gram of gelatin with stirring at 300 rpm for 2 h. Then, 100 mL of prewarmed DPBS was added for dilution. The resulting solution was dialyzed using a 10-kDa membrane (Spectrum Laboratories, Inc., Rancho Dominguez, CA, USA) at 37 °C for 5 days, filtered using a 0.2-μm filter, freeze-dried, and stored at −20 °C till use. Then, degree of functionalization (DOF) of the synthesized GelMA was determined by H^1 NMR spectroscopy (Fig. 2b). The peaks at δ = 2.9 ppm, corresponding to the protons of methylene of lysine in gelatin, and the peak at δ 7.5–8 ppm, corresponding to the aromatic amino acid moieties in gelatin, were used for DOF calculation [27,28]. DOF of GelMA prepared in the experiment was determined to be 69.3 ± 1.5 % according to the following equation (1):

$$DOF = \left[1 - \left(\frac{\int GelMA\ lysine / \int GelMA\ aromatic}{\int Gelatin\ lysine / \int Gelatin\ aromatic}\right)\right] \times 100\ (\%) \quad (1)$$

2.2.2. Fabrication of SN and DN hydrogels

Prepolymer solutions were prepared by dissolving 15 % GelMA for G15 and 1 % alginate and 15 % GelMA for A1G15 in a 0.15 M NaCl solution at 37 °C. Then, a photoinitiator (lithium phenyl-2,4,6-trimethylbenzoylphosphinate) was added to the pre-polymer solution at a concentration of 0.2 %. Therefore, the composition ratios (GelMA, alginate, and LAP) were 15:1:0.2 for A1G15 and 15:0:0.2 for G15. The precursor solution was transferred to various molds. To prepare flat hydrogel films (approximately 3 mm in thickness), 4 mL of the prepolymer solution was transferred to a 60 mm × 15 mm Petri dish. To prepare an anulus NGC, a conduit mold was assembled using a glass tube (inner diameter = 2.4 mm and thickness = 0.8 mm), stainless-steel rod (diameter = 1.2 mm), and custom-made 3D-printed thermoplastic polyurethane lids (Style-220; Cubicon, Seongnam, Republic of Korea) (Fig. S1). The rod was placed at the center of the glass tube and filled with the precursor solution; both ends were sealed with lids. The assembled molds were exposed to UV-A light (365 nm) for 1 min using a UV lamp (VL-215.LC; VILBER, Collégien, France) to crosslink the GelMA component [29]. Hydrogels were carefully retrieved from the mold. To prepare the DN hydrogel (i.e., A1G15), the samples were further incubated in sterile 0.9 M $CaCl_2$ solution for 5 min on a clean bench for secondary ionic crosslinking of the alginate component. Finally, the hydrogels were washed twice with sterile 0.15 M NaCl solution for 10 min each.

2.3. Characterization of NGCs

2.3.1. Scanning electron microscopy (SEM)

Internal microstructure of the hydrogel conduit was examined using SEM (Verios 5 UC; Thermo Fisher Scientific). Prior to SEM imaging, the conduit was freeze-dried and coated with a 9-nm platinum layer using a sputter coater (DSR1; VacCoat, London, UK). The pore wall thickness was measured from the SEM images using the ImageJ software (version 1.53a; National Institutes of Health, Bethesda, MD, USA).

2.3.2. Rheological and mechanical properties of NGCs

Rheological properties of the hydrogels were measured using an oscillatory rheometer (Kinexus Lab+; Malvern Instruments, Malvern, UK). Frequency sweep tests were performed in a 0.1–10 Hz frequency range with 0.5 % strain and a 3-mm gap using a 6-mm radius plate at 37 °C. The storage modulus was measured at 1 Hz in the frequency sweep tests. Mechanical properties were evaluated using a universal testing machine (TO-100-IC; Testone, Gyeonggi, Republic of Korea). For the tensile test, both ends of the 20-mm-long conduit were clamped and pulled with a 10 kN load cell at a rate of 5 mm min^{-1} until it broke. The ultimate tensile strength and elastic modulus of each sample were determined from the strain–stress curves (n = 5) as previously described [30]. Durability was assessed via successive compression of a 20-mm-long conduit with alternating 45 and 55 % strains at a rate of 80 mm min^{-1} for 100 cycles using the universal testing machine. Then, kink resistance was determined by bending a conduit with stainless-steel rods inserted at both ends and measuring the angle at which kinking occurred. For the suturability and fixation tests, one end of the conduit was secured with an 8-0 suture thread to form a suture loop 2 mm from the end, whereas the other end was clamped. The suture at the clamp was pulled at 5 mm min^{-1}. Suture retention force was determined as the strength at which the NGC broke (n = 4).

2.4. Preparation of ucMSC-laden NGCs

2.4.1. ucMSC culture

Human ucMSCs were used at passage number less than 8. ucMSCs were maintained in TCPs in growth medium (MEM alpha supplemented with 10 % FBS and 1 % antibiotic–antimycotic solution) in a humidified incubator with 5 % CO_2 at 37 °C. The medium was replaced every day. When the cells reached 80–90 % confluency, the cells were subcultured by treating 0.05 % trypsin/EDTA solution at 37 °C for 5 min. The cells were then collected by centrifugation at 1200 rpm for 5 min, resuspended in growth medium, and seeded onto new TCPs.

2.4.2. ucMSC encapsulation in hydrogel NGCs

The ucMSCs were encapsulated in various hydrogel NGCs according to the process described in section 2.2.2. The final hydrogel solution consisted of 15 % GelMA and 1 % alginate, mixed with MSCs at a density of 4 × 10^6 cells/mL. The DN hydrogel was prepared using 15 % (w/v) GelMA and 1 % (w/v) alginate, based on a previously established formulation that demonstrated excellent mechanical properties and regenerative efficacy in peripheral nerve repair models [16]. For cell encapsulation, a density of 4 × 10^6 cells/mL was selected to balance cellular activity and the structural integrity of the NGC. Notably, this cell density is comparable to previous studies using MSC-laden hydrogels for tissue regeneration [31,32]. In brief, all solutions were sterilized by autoclaving or syringe filtration (0.2 μm in pore size), and all procedures were performed in a clean biosafety bench. The ucMSCs were suspended in prepolymer solutions (0.01 w/v% $CaCl_2$ in saline) at a concentration of 4 × 10^6 cells/mL and transferred to an NGC mold. The mold was exposed to UV light for 1 min and subsequently incubated in sterile 0.9 M $CaCl_2$ solution for 5 min for secondary ionic crosslinking. The

ucMSC-encapsulated hydrogel sample was washed twice with sterile saline (0.15 M NaCl) for 10 min. The sample was transferred to a growth medium and incubated at 37 °C for subsequent experiments. To examine the distribution of the encapsulated ucMSCs in the hydrogel NGCs, the samples were stained. In brief, the samples were incubated in a 5 mM calcein AM solution in 10 mL DPBS at 37 °C with 5 % CO_2 for 10 min. Three-dimensional fluorescence images of the ucMSC-laden NGCs were acquired using a confocal laser-scanning microscope (FV3000RS; Olympus, Tokyo, Japan).

2.5. In vitro cell studies

2.5.1. Cell viability of encapsulated ucMSCs

Live/dead staining was performed according to the manufacturer's instructions (Thermo Fisher Scientific). Briefly, a staining solution was prepared by mixing 20 μL of EthD-1 (2 mM) and 5 μL of calcein AM (5 mM) with 10 mL of DPBS. The ucMSC-laden NGCs were incubated in a staining solution at 37 °C with 5 % CO_2 for 10 min and washed twice with DPBS for 5 min each. Fluorescence images were acquired using a fluorescence microscope (DMI3000 B, Leica, Wetzlar, Germany). Live (green) and dead (red) cells were counted from randomly selected images (n = 8). Cell viability was calculated using the following equation (2).

$$Cell\ viability\ (\%) = \left[\frac{Number\ of\ live\ cells}{Number\ of\ live\ cells + Number\ of\ dead\ cells}\right] \times 100 \quad (2)$$

2.5.2. Dorsal root ganglion (DRG) isolation

DRGs were isolated from 1-week-old Sprague–Dawley rats as previously described [33]. All isolation procedures were performed in a sterile environment on a clean bench. The rats were sacrificed, and their vertebral columns were separated and incubated in 4 °C DPBS. The surrounding muscles and fatty tissues were carefully removed, and the thoracic column was sagittally bisected. The spinal cord was then extracted. The DRGs located in the intervertebral foramina were carefully extracted with tweezers using a stereomicroscope (S6D; Leica, Wetzlar, Germany). The isolated DRGs were stored in 4 °C DMEM supplemented with 10 % FBS and 1 % antibiotic–antimycotic solution for subsequent experiments.

2.5.3. Direct co-culture of DRGs with ucMSC-laden NGCs

A 24-well plate was first coated with 300 μL of 0.05 % poly-L-lysine solution by incubation at 37 °C for 30 min and washed with DPBS. An isolated DRG explant was placed on the plate containing 100 μL of Neurobasal A media supplemented with 1 % GlutaMax, 2 % B-27 supplement, 1 % antibiotic–antimycotic solution, and 25 ng/mL NGF, followed by incubation in a humidified incubator at 37 °C with 5 % CO_2 for additional 30 min for attachment. ucMSC-laden NGC or cell-free NGC (14 mm in length) was transferred to a Transwell (a 3.0-μm pore size; SPL, Republic of Korea), which was further placed into the plate containing DRG. Subsequently, 1 mL of a 1:1 mixture of Neurobasal A medium and MEM Alpha was transferred to a Transwell plate and incubated for 48 h. For immunostaining, DRGs were fixed by incubating with 4 % paraformaldehyde solution for 30 min and permeabilized using 0.1 % Triton X-100 solution (in PBS) for 20 min. The samples were then incubated in the blocking solution (30 mg/mL bovine serum albumin in PBS) for 60 min and incubated in a primary antibody solution containing anti-neurofilament 200 (anti-NF200) polyclonal antibodies (1:100 in PBS) at 4 °C overnight. The samples were washed twice with PBS, incubated in a secondary antibody solution containing Alexa Fluor 555–conjugated donkey anti-rabbit IgG (1:200 in PBS) at 25 °C for 1 h, and washed twice with PBS. Fluorescent images were acquired using a fluorescence microscope (DMI3000B; Leica). Neurite length was measured as the distance from the DRG body to the tip of the neurite by analyzing random images using the NeuronJ plugin in ImageJ (n > 100).

2.5.4. Preparation of the conditioned medium (CM) from ucMSC-laden NGCs

14-mm long ucMSC-laden NGC and non-cell laden NGC were separately cultured in a 24-well plate with 800 μL of serum-free MEM alpha containing 1 % antibiotic–antimycotic solution for 3 days without changing the medium. After incubation, the medium was collected and centrifuged at 1500 rpm for 5 min to remove cell debris and filtered through a 0.2 μm pore size syringe filter. The resulting CM was stored at −80 °C until use.

2.5.5. Tube formation assay with the CM

HUVECs were used at passage number less than 6 in all experiments. HUVECs were maintained in ECM supplemented with 5 % FBS, 1 % penicillin–streptomycin, and 1 % endothelial cell growth supplement in a humidified incubator with 5 % CO_2 at 37 °C. The medium was replaced daily, and the cells were subcultured at 80 % confluence. For tube formation assay, HUVECs were cultured in serum-free medium for 12 h. Then, the cells were harvested by treating 0.05 % trypsin/EDTA solution at 37 °C for 5 min and seeded onto Matrigel-coated 24-well plates at a density of 1.2×10^5 cells per well. The cells were further cultured in a 1:1 mixture of serum-free ECM and each sample in a humidified incubator with 5 % CO_2 at 37 °C for 4 h. The tested sample groups included serum-free MEM alpha (control), CM from ucMSC NGC (MSC@NGC)), and CM from cell-free NGC (NGC). Optical images were acquired using a microscope (DM IL LED; Leica). The total numbers of branching points and closed loops in each group were measured from randomly selected optical micrographs using the ImageJ software.

2.5.6. In vitro RAW cell culture and cytokine quantification

RAW 264.7 macrophages were maintained in DMEM supplemented with 10 % FBS on TCP at 37 °C with 5 % CO_2. RAW cells were seeded in 24-well plates at a density of 10^5 cells/cm^2 and cultured in serum-free DMEM medium for 12 h. The RAW cells were cultured in a 1:1 mixture of serum-free M1 induction medium (DMEM containing 50 ng/mL LPS) and each sample for 24 h, and the medium in each group was collected. The sample groups included serum-free MEM alpha (control), ucMSC NGC CM (MSC@NGC)), and cell-free NGC CM (NGC). Inflammatory cytokines (i.e., TNFα and IL-6) in each collected medium were quantified using enzyme-linked immunosorbent assay (ELISA) kits (Invitrogen), according to the manufacturer's protocols.

2.5.7. Analysis of the encapsulated ucMSC secretomes

Human Growth Factor Array C1 (Raybiotech, GA, USA) was used to profile the secretome components in the CM from the culture of ucMSC-laden NGCs according to the manufacturer's instructions. In brief, the membrane was blocked with a blocking buffer at room temperature for 30 min and incubated with the CM at room temperature on a shaker for 2 h. Then, the membranes were incubated with a Biotinylated Antibody Cocktail on a shaker at 4 °C overnight and subsequently incubated with HRP-Streptavidin solution at room temperature for 2 h. Finally, the membrane was incubated in 500 μL detection buffer at room temperature for 2 min. Medium without ucMSCs was used as the control. Chemiluminescence images of the sample were acquired using the ChemiDoc XRS + System (Bio-Rad, Hercules, CA, USA), and the signal intensity of each protein was quantitatively analyzed with Image Lab software (version 6.1.0; Bio-Rad). The results were expressed as the relative ratio (%) between the positive and reference dot intensities.

2.6. In vivo studies

2.6.1. Surgical processes

Eight-week-old male Sprague–Dawley rats (180–200 g) were obtained from Damool Science (Daejeon, Republic of Korea). A sciatic nerve defect model was established as previously described [34]. All experimental procedures were reviewed and approved by the Committee on Animal Research and Ethics at the Gwangju Institute of Science

and Technology (GIST) Laboratory Animal Resource Center, Republic of Korea (approval number: GIST-2023-032). The rats were anesthetized with isoflurane (Hanapharma, Seoul, Republic of Korea). The right hip joint of each rat was dissected to expose the sciatic nerve, and a 10-mm defect was created. Each nerve end was placed in a 14-mm-long NGC and secured to the epineurium using 8-0 silk sutures. The biceps femoris muscle was closed using 6-0 silk sutures, and the skin was closed using 3-0 silk sutures. For autograft control, a 10-mm segment of the nerve was excised and reconnected to the distal and proximal ends using 8-0 silk sutures. The experimental groups included sham, autograft, non-cell laden NGC (Non-MSC), ucMSC-laden NGC (MSC), and a medical silicone conduit (Jiajie Rubber and Plastic, Shenzhen, China). Four rats were used in sham group and six rats were used in other group (n = 6). The rats were sacrificed with CO_2 at 6- and 12-weeks after surgery and treatment for subsequent analyses.

2.6.2. Sciatic nerve function evaluation

Sciatic nerve function recovery was evaluated by walking track analysis. The rats were allowed to freely walk on white paper, leaving footprints at 2, 4, 6, 9, and 12 weeks after surgery and treatment. Three parameters (i.e., print length (PL), toe spread (TS), and intermediate toe spread (IT)) were measured from the footprints of the operated (surgical) and non-operated (normal) sides. These parameters were used to calculate the sciatic functional index (SFI) using the following equation (3):

$$SFI = -38.8 \times \frac{EPL - NPL}{NPL} + 109.5 \times \frac{ETS - NTS}{NTS} + 13.3 \times \frac{EIT - NIT}{NIT} - 8.8 \quad (3)$$

where EPL is the PL of the operated side, NPL is the PL of the non-operated side, ETS is the TS of the operated side, NTS is the TS of the non-operated side, EIT is the IT of the operated side, and NIT is the IT of the non-operated side. An SFI value of 0 indicates normal nerve function, whereas an SFI value of −100 indicates the total loss of nerve function [35]. Measurements were performed by three independent blinded examiners.

2.6.3. Electromyography (EMG) signal recording

EMG signals were recorded from the gastrocnemius muscles using the Biopac MP36 system (Biopac Systems, Inc., Goleta, CA, USA) with a concentric needle electrode while stimulating the proximal part of the sciatic nerve of each experimental group with a Plexiglas-platinum electrode with a 1-ms pulse stimulus (1.5 V and 1 Hz). The recorded EMG signals were further analyzed to determine the peak-to-peak voltage after each electrical stimulus and evaluate the electrical activity of the gastrocnemius muscles using the Biopac Student Lab software (version 4.1.2; Biopac Systems, Inc.) [10,36].

2.6.4. Thermal paw withdrawal test

Thermal withdrawal response of experimental rats was assessed as previously described [37,38]. Briefly, right paw of each animal was placed in 60 °C water, and a video was recorded to measure the reaction time during the experiment. Reaction time was defined as the time between the paw's contact with hot water and its withdrawal from the water.

2.6.5. Gastrocnemius muscle evaluation

Gastrocnemius muscles from the left and right sides were collected at 6- and 12-weeks after surgery. The samples were rinsed with PBS and weighed. Then, muscle weight was measured, and muscle weight ratio was calculated by comparing the weights of the operated (right) and non-operated (left) muscles of each animal. For histological evaluation, muscle tissues were fixed by incubation in 4 % paraformaldehyde at 4 °C for 24 h, washed twice with PBS for 5 min each, embedded with paraffin, and sectioned into 10-μm thick slices using a microtome (RM2235; Leica). Masson's trichrome staining was performed, according to manufacturer's instructions (BBC Biochemicals). Masson's trichrome staining images were acquired using an optical microscope (DM-IL LED; Leica). The area of each muscle fiber (red) was measured, and the ratio of the fibrotic collagen area (blue) to the total muscle area (red) was determined from the Masson's trichrome staining images (n = 5) using the ImageJ software [39–41].

2.6.6. Morphometric analysis of the regenerated nerves

At 6- and 12-weeks after surgery and treatment, sciatic nerves were harvested, fixed overnight with 2.5 % glutaraldehyde solution at 4 °C for 24 h, and washed twice with PBS for 5 min each. Then, the samples were embedded in LR White Resin (EMS, Hatfield, PA, USA), sectioned into ultrathin slices (80 nm in thickness), and stained with lead citrate and uranyl acetate. Transmission electron microscopy (TEM) images were acquired using a transmission electron microscope (JEM-2100F; JEOL Ltd., Tokyo, Japan). Myelin sheath thickness and axon diameter were measured from at least three randomly selected TEM images using the ImageJ software. Finally, G-ratio was calculated using the following equation:

$$\text{G ratio} = \frac{\text{axon diameter}}{\text{single nerve fiber diameter}} \quad (4)$$

Single nerve fiber diameter was defined as the sum of the axon diameter and myelin sheath thickness [42].

2.6.7. Immunohistochemical analysis of the regenerated nerves

Harvested nerve tissues were fixed by incubation in 4 % paraformaldehyde at 4 °C for 24 h, washed twice with PBS for 5 min each, embedded with paraffin, and sectioned into 8-μm thick slices using a microtome. Then, the sections were permeabilized with 0.1 % Triton X-100 in PBS at room temperature for 10 min, blocked with 3 % goat serum in PBS at room temperature for 1 h, and incubated overnight at 4 °C with a primary antibody solution (anti-NF-200 polyclonal antibodies [1:100] and anti-S-100 monoclonal antibodies [1:100] in 1.5 % goat serum and 0.05 % Triton X in PBS). After washing twice with PBS, the sections were incubated with the secondary antibody solution (Alexa Fluor 555-conjugated donkey anti-rabbit IgG [1:200] and Alexa Fluor 488-conjugated donkey anti-mouse IgG [1:200] in PBS) at 37 °C for 1 h. To further reduce autofluorescence, the sections were incubated with 0.2 % Sudan Black B (in 70 % ethanol) for 2 h. Nuclei were stained with the DAPI solution (1:1000 in PBS). Fluorescence images were obtained using a fluorescence microscope. S-100- and NF-200-stained areas were quantified from randomly selected fluorescence images (n = 5) using the ImageJ software.

2.7. Statistical analyses

All experiments were performed at least in triplicate (n > 3), and results are expressed as the mean ± standard deviation, unless otherwise stated. Statistical significance was analyzed using a one-way analysis of variance, followed by Tukey's post-hoc comparison of the mean values. Statistical analyses were performed using Origin Pro 9.3 (OriginLab Corp., Northampton, MA, USA). Statistical significance was determined at $p < 0.05$.

3. Results and discussion

3.1. Preparation of GelMA/alginate DN hydrogel NGCs

DN hydrogel NGC (A1G15) was fabricated via a two-step process with 1 % alginate and 15 % GelMA: i) UV photopolymerization and ii) ionic crosslinking with calcium ions (Fig. 2a). On the other hand, SN hydrogel NGC (G15) was fabricated as a control using 15 % GelMA and UV photopolymerization. Synthesis of GelMA was confirmed via ^1H

NMR spectroscopy (Fig. 2b). DOF of the synthesized was 69.3 ± 1.5 %. Hydrogel NGCs were fabricated using a laboratory-made assembly mold (Fig. S1). Annulus DN and SN NGCs of 1 cm length, 1.2 mm inner diameter, and 0.6 mm wall thickness were successfully fabricated. G15 was transparent, whereas A1G15 was slightly milky, likely due to the ionic crosslinking of the alginate chains with calcium ions (Fig. 2c) [43]. FT-IR spectroscopy was performed to confirm DN structure formation on three A1G15 hydrogel types: non-crosslinked, photo-crosslinked, and photo- and ionic-ally crosslinked samples (Fig. S2). The non-crosslinked sample exhibited characteristic GelMA peaks at 3311 cm^{-1} (O–H/N–H stretching), 1645 cm^{-1} (C=O stretching and methacrylate C=C), 1529 cm^{-1} (amide II) and 1232 cm^{-1} (amide III) [44–47]. After photo-crosslinking, the intensity of 1645 cm^{-1} peak decreased, indicating methacrylate consumption and covalent network formation. In the DN hydrogel, asymmetric and symmetric carboxylate peaks appeared at 1633 and 1440 cm^{-1}, respectively. Notably, these peaks were slightly red-shifted (~2 cm^{-1}) compared to the photo-crosslinked sample, suggesting Ca^{2+}-mediated ionic crosslinking of alginate. Although alginate signals were weak due to its low content, these spectral shifts combined with enhanced mechanical properties (Fig. 3) confirm successful DN hydrogel formation. SEM images showed that both the SN and DN NGCs had typical hydrogel microstructures with internal pores that can facilitate efficient nutrient and waste transport (Fig. 2d). Interestingly, DN hydrogels had pore walls (13.7 ± 7.1 μm) 1.7-times thicker than the SN hydrogels (8.2 ± 3.4 μm) (Fig. 2e), indicating a denser network in DN NGC. The thick pore walls observed in the SEM images are generally indicative of enhanced mechanical properties and dense hydrogel networks [16,48].

3.2. Mechanical properties of hydrogel NGCs

For robust and efficient PNI recovery, hydrogels with appropriate mechanical properties, such as strength and fatigue resistance, are required. As peripheral nerves are located just beneath the skin or around highly mobile joints and experience repeated elongation and relaxation, mechanical protection of regenerating nerves is important [12,49]. Traditional hydrogels are soft and weak and considered unsuitable as NGC materials. In contrast, DN hydrogels can demonstrate superior mechanical properties, fatigue resistance, and suture retention, which are beneficial for the protection and long-term stability of the regenerating peripheral nerves. In this study, rheological and mechanical characteristics of SN G15, SN A1G15 (photopolymerized but non-ionic crosslinked), and DN A1G15 (photopolymerized followed by a second ionic crosslinking) were investigated. First, SN A1G15 (6.4 ± 1.3 kPa) exhibited a lower storage modulus than G15 (23.6 ± 3.0 kPa), possibly because of the interference of alginate polymer chains with the formation of the GelMA network in A1G15 during UV crosslinking (Fig. 3a; Fig. S3). Conversely, after calcium treatment for secondary ionic crosslinking, DN A1G15 exhibited a significantly increased modulus of 35.5 ± 3.0 kPa, which was 1.5- and 5.5-fold higher than those of SN G15 and non-ionically crosslinked SN A1G15, respectively, indicating enhanced mechanical properties attributed to the ionic crosslinking network of the alginate chains. Furthermore, mechanical characteristics of SN G15, SN A1G15, and DN A1G15 hydrogels were examined using tensile stress–-strain curves (Fig. 3b). The ultimate tensile strengths of SN G15 (63 ± 26 kPa) and SN A1G15 (79 ± 15 kPa) were not significantly different. DN A1G15 exhibited the highest tensile strength (173 ± 62 kPa) (Fig. 3c). In

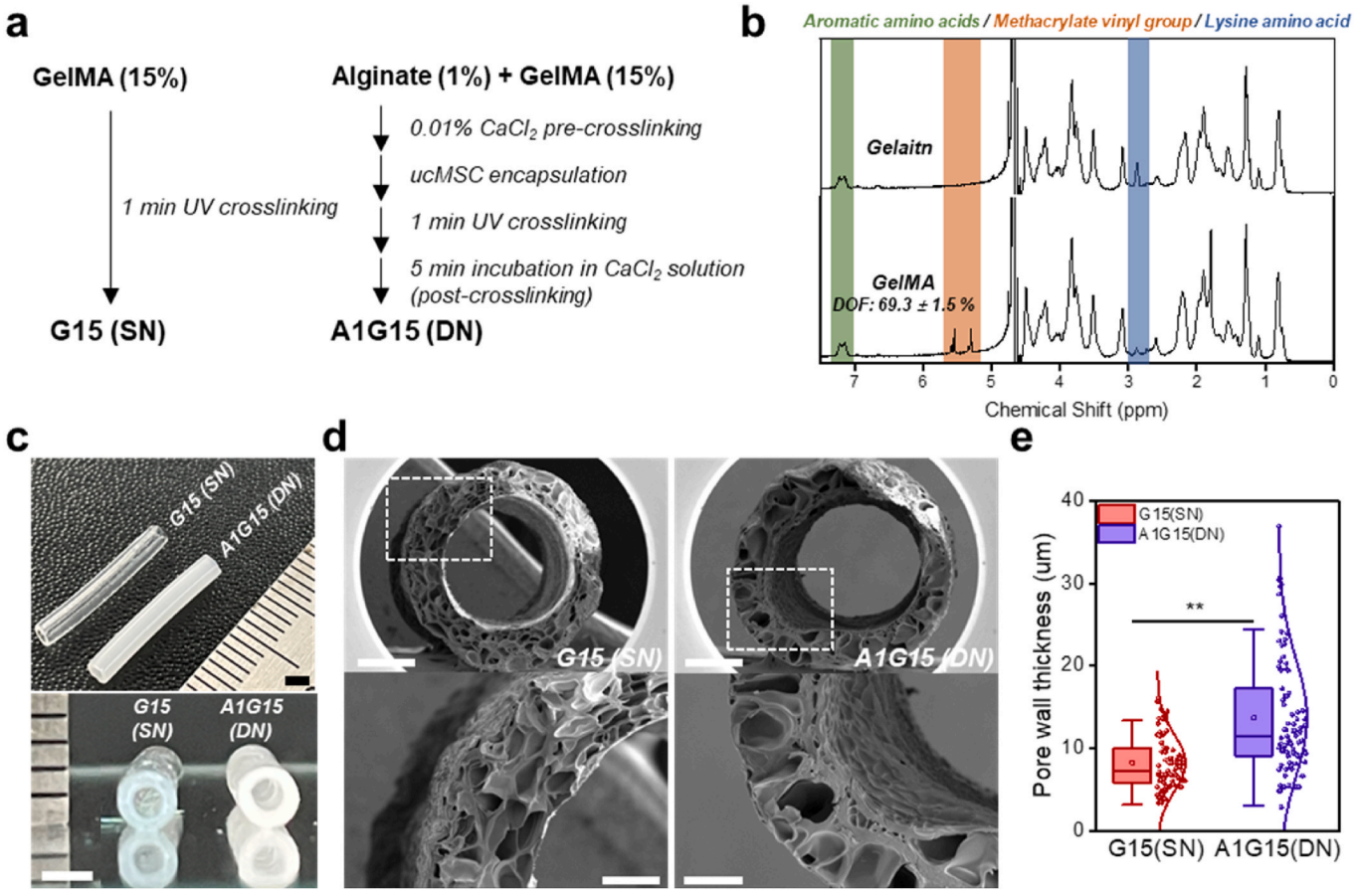

Fig. 2. Fabrication of gelatin methacrylate (GelMA)/alginate DN NGCs. (a) Fabrication processes of single-network (SN) GelMA (G15) and DN GelMA/alginate (A1G15) NGCs. (b) ^{1}H NMR spectra of gelatin and GelMA. (c) Photographs of G15 and A1G15 NGCs with side and cross-sectional views. Scale bars = 2 mm. (d) Cross-sectional scanning electron microscopy (SEM) images of G15 and A1G15 NGCs. Scale bars = 500 μm (top) and 300 μm (bottom). (e) Pore wall thicknesses of G15 and A1G15 NGCs (n > 80; **p < 0.01).

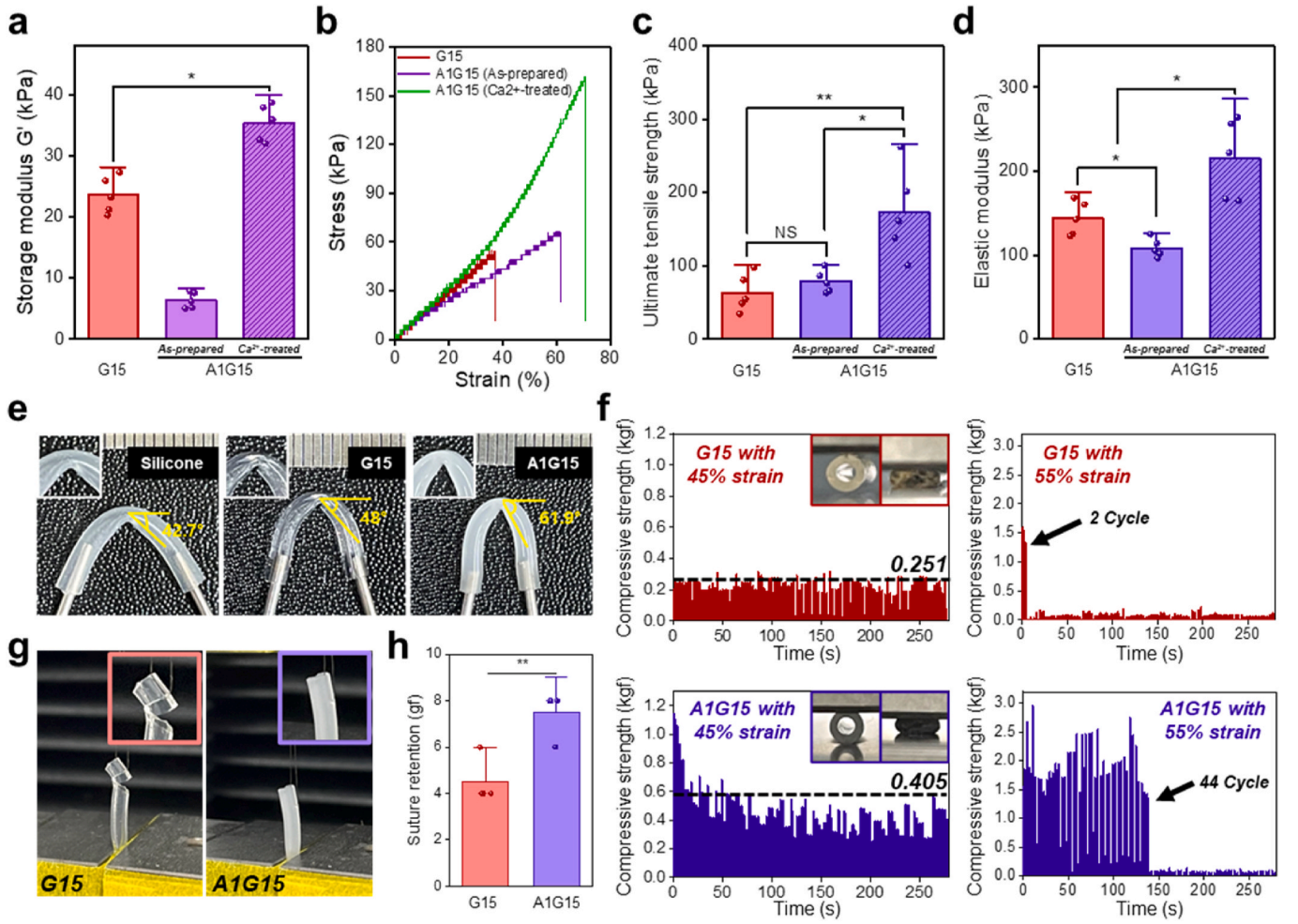

Fig. 3. Rheological and mechanical properties of hydrogel-based NGCs. (a) Storage moduli (G′) of SN G15, SN A1G15, and DN A1G15 (n = 5; *p < 0.05). Storage modulus was obtained at 1 Hz in the frequency sweep test. (b) Tensile stress–strain curves of SN G15, SN A1G15, and DN A1G15. (c) Ultimate tensile strength and (d) elastic moduli of SN G15, SN A1G15, and DN A1G15 obtained from the tensile stress–strain curves (n = 5; *p < 0.05; **p < 0.01). (e) Photographs of the medical silicone conduit, SN G15, and DN A1G15 NGCs at their respective critical bending angles. (f) Successive compression of SN G15 and DN A1G15 at 45 and 50 % strain during 100 cycles. (g) Suture retention tests of SN G15 and DN A1G15. Photographs were acquired at the breaking point of SN G15 (approximately 6 % strain). (h) Suture retention forces of SN G15 and DN A1G15 (n = 4; **p < 0.01).

addition, the elastic modulus of DN A1G15 (215 ± 48 kPa) was significantly higher than those of SN G15 (144 ± 20 kPa) and SN A1G15 (108 ± 11 kPa) (Fig. 3d). Compression test revealed trends similar to those observed in the tensile tests. For example, ultimate compressive strength of DN A1G15 (439 ± 146 kPa) was 1.7-times higher than that of SN G15 (255 ± 89 kPa) (Fig. S4). Although the alginate concentration in the DN hydrogel was relatively low (1 % w/v), incorporated alginate can form an ionically crosslinked secondary network that can significantly enhances mechanical strength. This alginate network can act synergistically with the covalently crosslinked GelMA network to provide efficient stress dissipation and energy distribution.

Kink-resistance test was performed to determine the maximum bending angle at which the hollow lumen of the NGC remained unobstructed (Fig. 3e). Appropriate kink resistance of an NGC is crucial to ensure the protection of regenerating nerves in dynamic environments [50]. DN A1G15 NGC exhibited excellent kink resistance. Critical bending angle was 42.7° for medical silicone conduit, 48.0° for SN G15, and 61.9° for DN A1G15. Superior kink resistance of the DN hydrogel NGC indicated its suitability for maintaining an open lumen, thereby preventing nerve regeneration failure in highly mobile tissues, such as the elbow, knee, and finger joint tissues. Notably, the developed DN hydrogel NGCs exhibited better kink resistance than the commercially available collagen-based NGCs, such as NeuraGen® (approximately 55°) and Neuroflex® (approximately 60°), and other conventional non-flexible or silk fibroin NGCs [50–53]. As fatigue resistance and durability are also essential for high NGC performance, we conducted cyclic compression of the SN G15 and DN A1G15 NGCs and examined their mechanical stability. After 100 cycles under 45 % strain, the compressive strength of A1G15 (0.405 kgf) was significantly higher than that of G15 (0.251 kgf). In additional tests under more rigorous conditions with 50 % strain for 100 cycles, SN G15 failed after only two cycles, whereas DN A1G15 maintained its mechanical strength for up to 44 cycles, demonstrating that DN A1G15 NGC exhibited excellent fatigue resistance and durability. Suturability is desirable for the practical use of NGCs. Hence, suture retention test was performed to determine that each NGC could endure without breaking when subjected to 8-0 suture. A1G15 exhibited 1.67-fold higher suture retention strength (7.5 ± 1 kgf) than G15 (4.5 ± 1 kgf). Collectively, these findings suggest that DN A1G15 possesses excellent mechanical properties, including kink resistance, fatigue resistance, and suture retention, suitable for NGC implantation.

3.3. Regenerative potential of the encapsulated ucMSCs in vitro

The distribution and viability of the ucMSCs encapsulated within NGCs were assessed by calcein-AM staining and confocal microscopy (Fig. 4a and Video S1). Viable (green) ucMSCs were uniformly

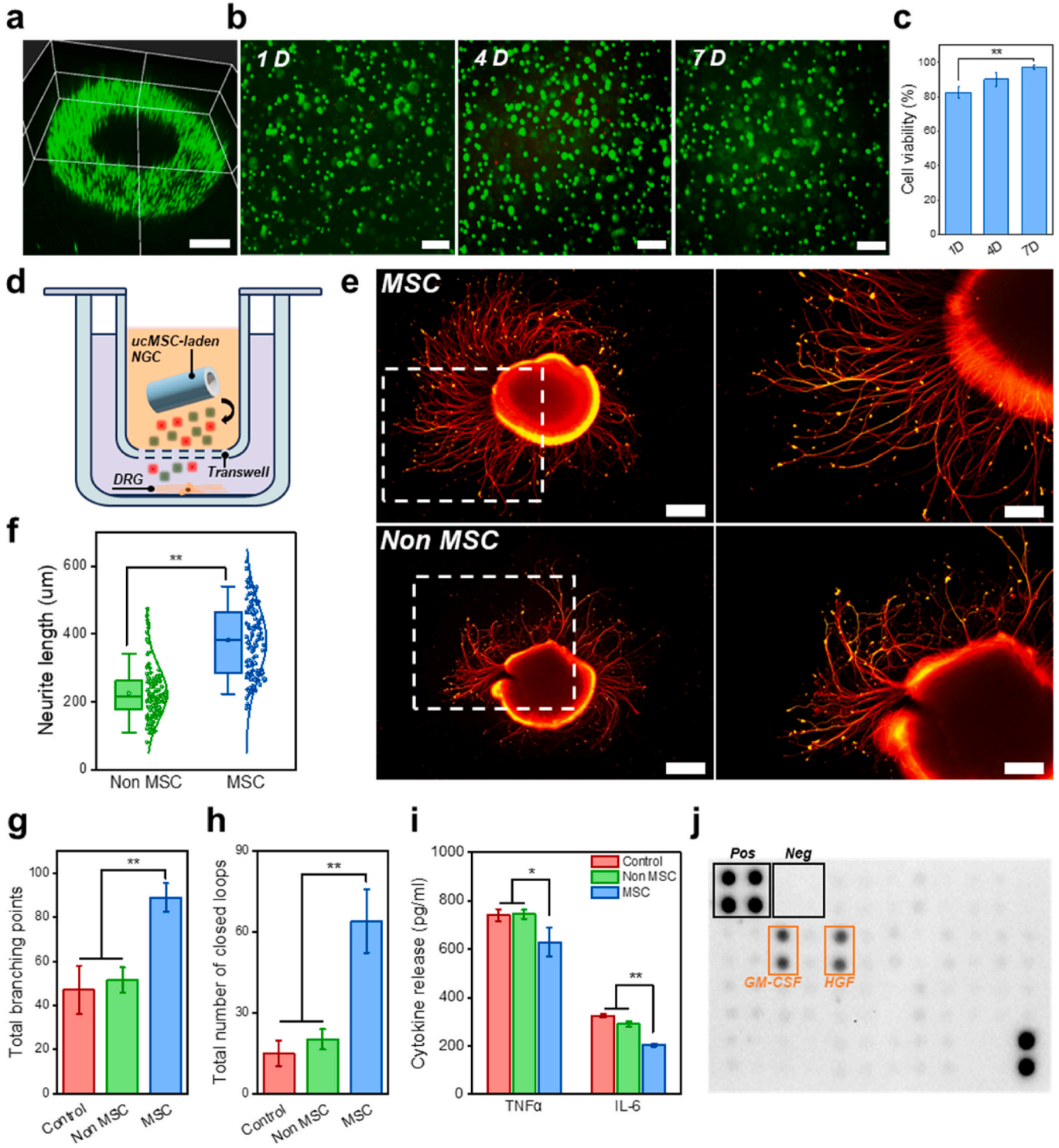

Fig. 4. In vitro studies to characterize the efficiency of ucMSC-laden NGCs in peripheral nerve regeneration. (a) Confocal image of ucMSCs encapsulated in A1G15 NGC. Scale bar = 500 μm. (b) Live/dead images of ucMSCs encapsulated in A1G15 NGC. Fluorescence images were acquired on days 1, 4, and 7. Scale bar = 100 μm. (c) Cell viability of encapsulated ucMSCs after incubation for seven days (n = 8; **p < 0.01). (d) In vitro co-culture of NGCs and dorsal root ganglion (DRG) using a Transwell. Samples included cell-free A1G15 NGCs (Non-MSC) and MSC-laden A1G15 NGCs (MSC). (e) DRG explants stained for NF-200 (red) after 48 h of co-culture. Scale bars = 200 μm (left) and 100 μm (right). (f) Neurite lengths of DRG explants cultured with cell-free NGCs or MSC-laden NGCs (n > 100; **p < 0.01). (g) Total branching points and (h) total number of closed loops for human umbilical vein endothelial cells (HUVECs). HUVECs were cultured with the control (medium) or conditioned medium (Non-MSC or MSC groups) for 4 h (n = 4 per group; **p < 0.01). (i) Quantification of tumor necrosis factor (TNF)-α and interleukin (IL)-6 levels in various culture media. RAW cells were cultured in the medium (control) or conditioned medium (Non-MSC or MSC groups) for 24 h (n = 3; *p < 0.05; *p < 0.05). (j) Antibody array analysis of human growth factors in a conditioned medium with ucMSC-laden A1G15 NGCs.

distributed throughout the NGC matrix. The encapsulated ucMSCs retained high cell viability with >80 % up to 7 days (Fig. 4b and c), indicating cytocompatibility of the materials and procedures for ucMSC-laden NGC fabrication. Additionally, the metabolic activity of ucMSCs in NGCs gradually increased from days 1–7, suggesting appropriate proliferation (Fig. S5).

MSCs secrete various neuro-regenerative factors, including glial cell-derived neurotrophic factor, NGF, brain-derived neurotrophic factor, and neurotrophin-3 (NT-3) [54]. Hence, the neuroregenerative potential of the encapsulated ucMSCs was assessed by a co-culture of DRG with either ucMSC-laden NGCs (MSC group) or NGCs without MSCs (non-MSC group) (Fig. 4d). The DRGs in the MSC group exhibited significantly longer neurite outgrowth (381 ± 106 μm) compared to the non-MSC group (225 ± 78 μm) after 48 h of co-culture (Fig. 4e and f). These results imply paracrine effects of the encapsulated ucMSCs on the promotion of neurite growth, confirming the neurogenic potential of ucMSCs via neurotrophic factor secretion. Similarly, the DRG cultured in CM of the MSC group showed a 1.5-fold longer neurites (433 ± 92 μm) compared to that of the non-MSC group (228 ± 54 μm) (Fig. S6). Furthermore, we cultured primary rat Schwann cells in CM from MSC-laden DN NGCs (Fig. S7). Schwann cells cultured in CM MSC-laden DN NGCs exhibited significantly enhanced migration compared to those cultured in CM from MSC-free NGCs, indicating that the MSCs encapsulated in the DN hydrogels promoted Schwann cell migration via paracrine signaling.

Microvessels are crucial components for peripheral nerve tissue regeneration, nutrient and oxygen delivery, and waste removal [55,56]. MSCs promote vascular formation by secreting various angiogenic factors, such as vascular endothelial growth factor (VEGF) and platelet-derived growth factor (PDGF) [57]. The angiogenic potential of the encapsulated ucMSCs was assessed by a tube formation assay (Fig. 4h and Fig. S8). After 4 h of incubation in CM, the total branching points and closed-loop numbers of the HUVECs were examined. Interestingly, the MSC group exhibited significantly more branching points (Fig. 4g) and closed loops (Fig. 4h). This promotion of angiogenesis can be attributed to the production of proangiogenic factors by the encapsulated ucMSCs. NGC implantation can also cause foreign body reactions and inflammation, which can hinder effective functional nerve regeneration [58–60]. Hence, several efforts have been made to provide anti-inflammatory substances to attenuate inflammation and promote nerve regeneration [61,62]. In general, MSCs possess unique immunomodulatory abilities that can mitigate excessive inflammatory reactions. Such immunomodulatory ability of encapsulated ucMSCs was assessed by quantifying pro-inflammatory cytokines (i.e., TNFα and IL-6) in medium cultured with macrophages and CM for 24 h the TNFα concentration in the MSC group (628 ± 60 pg/mL) was found statistically lower than in the non-cell group (743 ± 18 pg/mL) and the negative control (739 ± 25 pg/mL). Similarly, the MSC group (203 ± 7 pg/mL) produced a significantly smaller amount of the IL-6 than non-cell (290 ± 11 pg/mL) and the negative control (324 ± 8 pg/mL) groups (Fig. 4i). These results suggest the anti-inflammatory ability of the encapsulated ucMSCs. Finally, a human growth factor antibody array was used to profile the secretomes produced by the ucMSCs encapsulated in A1G15 (Fig. 4j). More growth factors were detected in the MSC group. For example, granulocyte macrophage colony-stimulating factor (GM-CSF) and hepatocyte growth factor (HGF) levels were approximately 59-fold and 19-fold higher, respectively, in the MSC group compared to those in the control group (Fig. S9). GM-CSF is a key modulator of post-injury immune responses and has been reported to accelerate early axonal regeneration in rat sciatic nerve injury models [63]. HGF plays a pivotal role in peripheral nerve repair by activating Schwann cells and enhancing neurite extension and axonal growth [64,65]. In addition, the MSC group exhibited increased levels of other regenerative factors, including heparin-binding EGF-like growth factor (HB-EGF), insulin-like growth factor binding protein 4 (IGFBP-4), and platelet-derived growth factors (PDGF-AA and PDGF-AB). These growth factors are involved in tissue regeneration processes, such as angiogenesis, cell proliferation, and matrix remodeling. Altogether, the results indicated that encapsulated uc-MSCs produced diverse bioactive factors that can enhance peripheral nerve regeneration.

3.4. *In vivo efficacy tests of ucMSC-laden NGCs in a rat sciatic nerve defect model*

For in vivo studies, 14-mm-long NGC and 10-mm sciatic nerve defect rat model were used. The experimental groups included i) sham ii) autograft (Auto) as a positive control, iii) medical-grade silicone conduit (Silicone) as a control, iv) non-cell-laden NGC (Non-MSC), and v) ucMSC-laden NGC (MSC) (Fig. S10). All NGCs were successfully implanted into the nerve defects and found to remain at the implanted sites for 6 weeks (Fig. 5a). At week 12, the hydrogel NGCs (Non-MSC and MSC) disappeared, whereas intact regenerating nerves were observed. It should be noted that non-degradable NGCs may require secondary surgeries for removal after complete nerve regeneration, whereas rapidly degrading NGCs cannot sufficiently support nerve reconnection [66]. Hence, NGCs with suitable degradation kinetics are highly desirable [67]. During 10-mm sciatic nerve gap regeneration with implanted NGCs, the axonal phase begins around two weeks post-surgery, where the first axons migrate from the proximal nerve end. Subsequently, the myelination phase occurs approximately four weeks post-surgery, during which Schwann cells produce myelin. Therefore, it is ideal for the NGC to begin gradually degrading thereafter [68]. Hematoxylin and eosin staining revealed that the DN hydrogel NGCs (Non-MSC and MSC) gradually degraded and mostly disappeared by 12 weeks, implying their suitable degradation kinetics for peripheral nerve regeneration (Fig. S11 and S12). To explore the degradation profile, the thickness of residual NGCs was measured at weeks 4, 8, and 12 post-implantation (Fig. S13). Gradually decrease in NGC thickness indicates that the DN hydrogel degrades in a rate compatible with peripheral nerve regeneration. A degradation rate matched to tissue healing may enhance therapeutic efficacy by supporting axonal growth and reducing long-term material persistence [66]. Future studies will incorporate non-invasive imaging methods, such as fluorophore labeling or MRI-based tracking, for more precise and real-time monitoring of hydrogel degradation in vivo. We previously observed that alginate/gelatin DN hydrogel NGCs prepared via gamma irradiation showed superior in vivo retention compared to SN gelatin NGCs [16]. For example, DN NGCs remain intact for 6 weeks in injured sciatic nerves. In addition, no significant symptoms of severe immune responses were observed at 12 weeks (Fig. S12).

Functional recovery of the regenerated sciatic nerve was assessed using walking analysis. Specifically, SFI was analyzed using footprint images (Fig. S14). The SFI gradually increased in all groups after surgery and treatment. At 2 weeks, the Auto and MSC groups had significantly higher SFI values than the Silicone group. Both groups presented higher SFI values than the Non-MSC and Silicone groups by week 4; however, the difference between the Auto and MSC groups was not significant. These results suggest that ucMSCs encapsulated in DN hydrogel NGCs promoted nerve regeneration in the early stages, comparable to the gold standard autograft. After 6 weeks, Auto group showed significantly higher SFI values than the MSC group. Nevertheless, SFI values in the MSC group were significantly higher than those in Non-MSC and Silicone groups. At 12 weeks, the SFI values in the individual groups were in the following order: Sham > Auto > MSC > Non-MSC > Silicone (Fig. 5b). For example, the SFI values of Sham, Auto, MSC, Non-MSC, and Silicone groups were −9 ± 3, −61 ± 4, −72 ± 4, −85 ± 1, and −90 ± 1, respectively (Fig. 5c). To better understand the performance of our MSC-laden DN hydrogel NGCs, we compared our SFI results with those reported in the literature for other natural and synthetic polymer-based NGCs. Our NGC demonstrated superior regenerative performance compared to NGCs made from silk fibroin [69], collagen, chitosan [70], polycaprolactone (PCL) [70] and poly(L-lactide-co-ε-caprolactone) (PLCL) [71,72]. Furthermore, our system was superior to other stem

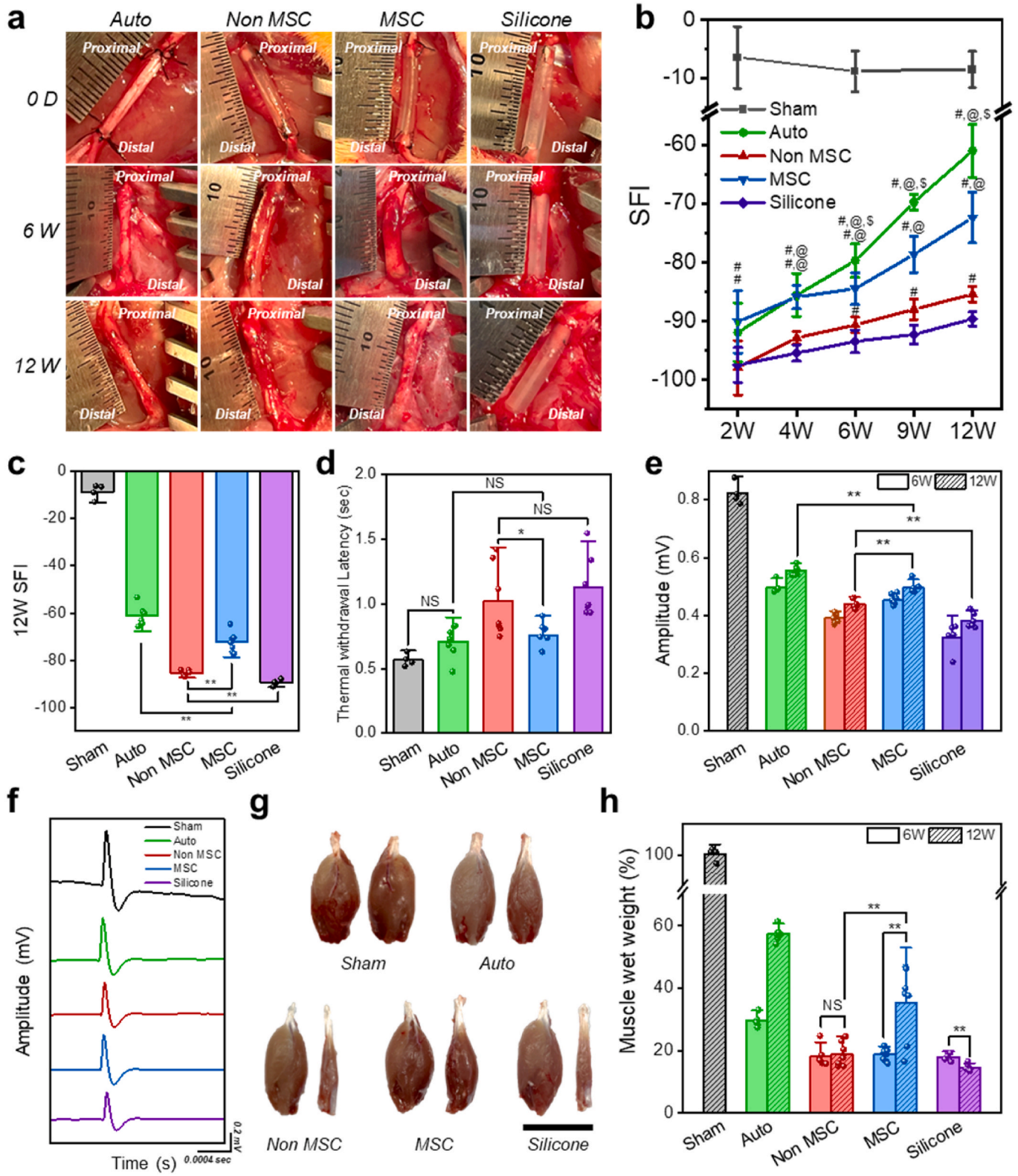

Fig. 5. In vivo peripheral nerve regeneration in a sciatic nerve defect model using various NGCs. Experimental groups included sham, autograft (Auto), medical grade silicone conduit (Silicone), non-cell-laden NGC (Non-MSC), and ucMSC-laden NGC (MSC) groups. (a) Images at 0 d, 6 weeks, and 12 weeks after surgery and NGC implantation. (b) Sciatic functional index (SFI) at weeks 2, 4, 6, 9, and 12 (#$p < 0.05$ vs. silicone group in the same week; @$p < 0.05$ vs. non-MSC group in the same week; \$$p < 0.05$ vs. MSC group in the same week). (c) SFI at 12 weeks after surgery and treatment ($n = 6$; **$p < 0.01$). (d) Thermal withdrawal latency at 12 weeks ($n = 6$; *$p < 0.05$). (e) Onset-to-peak amplitudes at weeks 6 and 12 ($n = 6$; **$p < 0.01$). (f) Electromyograms 12 weeks after surgery. (g) Photographs of gastrocnemius muscles (surgery [right] and non-surgery [left]). Scale bar = 25 mm. (h) Muscle wet weight ratio of gastrocnemius muscles at weeks 6 and 12 ($n = 6$; **$p < 0.01$).

cell-based conduits, including those incorporating bone marrow- or adipose-derived MSCs within Matrigel or fibrin–collagen hydrogels in similar sciatic nerve defect models [73,74].

As an additional functional evaluation, the thermal paw withdrawal test was performed to compare the recovery of sensory and motor functions by measuring the pain response in each group. At 12 weeks, the thermal withdrawal latency of the Sham (0.57 ± 0.05 s), Auto (0.71 ± 0.12 s), and MSC (0.75 ± 0.10 s) groups was significantly lower than those of the Non-MSC (1.02 ± 0.28 s) and Silicone (1.12 ± 0.24 s) groups (Fig. 5d). These results indicate enhanced recovery of sensory and motor functions originating from the encapsulated ucMSCs. Electrophysiological functions of the regenerated sciatic nerves were assessed with respect to the EMG signal amplitude (Fig. 5e and f). The onset-to-peak amplitudes increased in all groups after surgery. These amplitudes at 12 weeks were in the order of the Sham (0.82 ± 0.04 mV), Auto (0.56 ± 0.02 mV), MSC (0.5 ± 0.02 mV), Non-MSC (0.33 ± 0.02 mV), and Silicone (0.38 ± 0.02 mV) (Fig. 5e and f). These results indicated that ucMSC-laden NGCs promoted the recovery of electrophysiological functions in the regenerating sciatic nerve. Nerve conduction velocity (NCV) was measured at 12 weeks post-implantation to evaluate functional integration. No significant differences in NCV were observed among the experimental groups, which may be attributed to the reestablishment of nerve connection in all groups despite differences in regenerated nerve diameter (Fig. S15). Sciatic nerve injury can lead to skeletal muscle atrophy, which results in reduced muscle mass, decreased strength, and impaired mobility [75]. The extent of muscle atrophy was assessed by examining the weight ratios of the right (surgical) and left (non-surgical) gastrocnemius muscles at 6 and 12 weeks (Fig. 5g). At 6 weeks, significant muscle atrophy was observed in all groups, in which the Auto group showed the highest muscle weight ratio. Interestingly, only the Auto and MSC groups showed 2.0- and 1.9-fold increases in muscle weight ratios, respectively, whereas the Non-MSC and Silicone groups showed no improvement. The MSC group showed higher muscle weight ratios than the Non-MSC and Silicone groups at 12 weeks. For example, muscle weight ratios of the Sham, Auto, MSC, Non-MSC, and Silicone groups were 100.2 ± 2.1, 57.3 ± 2.2, 35.2 ± 11.8, 18.8 ± 3.9, and 14.4 ± 1.1 %, respectively (Fig. 5h). Altogether, these findings suggest that ucMSC-laden NGC efficiently promoted nerve regeneration, mitigated gastrocnemius muscle atrophy, and enhanced muscle regeneration. Overall, significant functional recovery of injured nerves was observed by treatment of MSC-laden DN hydrogel NGC, as demonstrated by SFI, EMG, and thermal withdrawal latency tests, which are widely used methods for evaluating motor, electrophysiological, and sensory function in peripheral nerve injury models. Nevertheless, advanced techniques (e.g., dynamic gait analysis and compound muscle action potential recordings) would be valuable in future studies to provide deeper insights into functional restoration.

3.5. Histological analysis of the regenerated sciatic nerves

Sciatic nerve regeneration was further histologically assessed. First, sciatic nerve tissues obtained at week 12 were stained for S-100 and NF-200 as biomarkers for Schwann cells and neurons, respectively. Schwann cells play critical roles in peripheral nerve regeneration by producing trophic factors and cytokines, promoting nerve regeneration, and forming the Bands of Büngner, thereby creating tracks for axon elongation [76,77]. Neurofilaments are mature neuronal cytoskeleton proteins supporting the structural integrity and shape of neurons; higher expression levels of neurofilaments indicate better neuronal maturation [78,79]. Immunostaining at 12 weeks post-surgery revealed that the MSC group exhibited higher S-100 and NF-200 expression levels than the other NGC groups (Non-MSC and Silicone) (Fig. 6a). Quantitative analysis revealed that S-100 expression levels in the MSC group (51.9 ± 6.5 %) were lower than those in the Sham (84 ± 6.9 %) and Auto groups (76.4 ± 5.6 %) but significantly higher than those in the Non-MSC (41.2 ± 5.7 %) and Silicone (25.9 ± 9.0 %) groups (Fig. 6b). NF-200 expression levels exhibited similar trends. For example, NF-200-positive areas were 136.2 ± 15.7, 80.1 ± 4.1, 64.1 ± 5.0, 41.2 ± 3.0, and 36.3 ± 2.5 % in the Sham, Auto, MSC, Non-MSC, and Silicone groups, respectively (Fig. 6c). To further assess the spatial pattern of nerve regeneration within the conduit, immunofluorescence staining for S-100 and NF-200 was performed on transverse sections obtained from the proximal, central, and distal regions of the regenerated nerve (Fig. S16). The MSC-laden DN hydrogel group showed robust and continuous expression of both markers across all three regions, indicating progressive Schwann cell migration and axonal elongation along the conduit. In contrast, Non-MSC and Silicone groups showed weak intensities, particularly in the central and distal regions, indicating insufficient axonal regeneration and Schwann cell migration. These immunohistochemical analyses with NF-200 and S100 suggest that the MSC-laden DN hydrogel NGCs effectively promoted nerve regeneration and Schwann cell myelination, respectively. However, molecular-level analyses, such as qPCR and Western blotting, would be necessary as future studies to provide additional insights into gene and protein expression associated with nerve repair, including key neurotrophic and regeneration-associated markers.

Remyelination is essential for successful regeneration and nerve function as it facilitates rapid and efficient transmission of nerve signals and protects the neurons [80]. Appropriate nerve regeneration is commonly indicated by increased myelin sheath thickness and axon size. In our studies, TEM images of the distal regions of nerve tissues 12 weeks post-surgery revealed thick and dense myelin structures in the Auto and MSC groups. In contrast, Silicone group exhibited thin myelin sheaths and numerous vacuolar-like defects (Fig. 6d). Quantitative analysis of myelin sheath indicated that the Sham (1.26 ± 0.07 μm) and Auto groups (0.63 ± 0.03 μm) had the thick myelin. Myelin thickness in the MSC group (0.43 ± 0.04 μm) was significantly higher than those in the Non-MSC (0.34 ± 0.04 μm) and Silicone (0.32 ± 0.04 μm) groups) (Fig. 6e). A similar trend was observed for axon diameter, with Sham (3.39 ± 0.2 μm) > Auto (2.13 ± 0.14 μm) > MSC (1.8 ± 0.13 μm) > Non-MSC (1.56 ± 0.11 μm) ≈ Silicone (1.48 ± 0.08 μm) groups (Fig. 6f). G-ratio, defined as the ratio of the inner to outer myelin sheath, was obtained and compared to assess the myelin thickness and nerve conduction efficiency [42]. A low G-ratio indicates excessively thick myelin, which leads to inefficient space utilization and reduced nerve conduction velocity. Conversely, a high G-ratio indicates excessively thin myelin, which causes insufficient axonal protection and reduced nerve conduction velocity. The optimal G-ratio is generally considered to be approximately 0.6 to for balanced characteristics between the axon size and myelin thickness [81]. Sham (0.55 ± 0.02) and Auto groups (0.56 ± 0.02) exhibited values closest to the optimal G-ratio, followed by the MSC group (0.67 ± 0.02). In contrast, G-ratios of the Non-MSC (0.69 ± 0.02) and Silicone (0.69 ± 0.02) groups largely deviated from 0.6 and were significantly higher than that of the MSC group (Fig. 6g).

Human nuclear antigen (HNA) staining was performed on nerve tissues 12 weeks post-surgery to determine the residence and distribution of transplanted ucMSCs in the DN NGCs. HNA-positive cells, indicating the transplanted MSCs, were rarely observed in the nerve tissues, likely due to DN hydrogel degradation and cell migration (Fig. S17). Nevertheless, some HNA-positive cells were observed, especially in the epineurium, but not in the nerve fascicle. While the number of residual ucMSCs was insufficient for phenotypic analysis, their presence indicates a potential contribution to the regenerative process. Notably, over 80 % of transplanted MSCs encapsulated within NGCs remained viable at 1 week post-implantation (Fig. S18), indicating that the MSCs may contribute to at least the early stages of nerve regeneration.

Microvessels facilitate the supply of nutrients and oxygen and guide Schwann cells to reconnect the severed nerves during nerve regeneration [55,82]. von Willebrand factor immunostaining indicated well-structured and more blood vessels in the nerve tissues of the Auto and MSC groups at 12 weeks (Fig. S19). This result is consistent with those of the in vitro culture of HUVECs (Fig. 4g and h) and growth factor

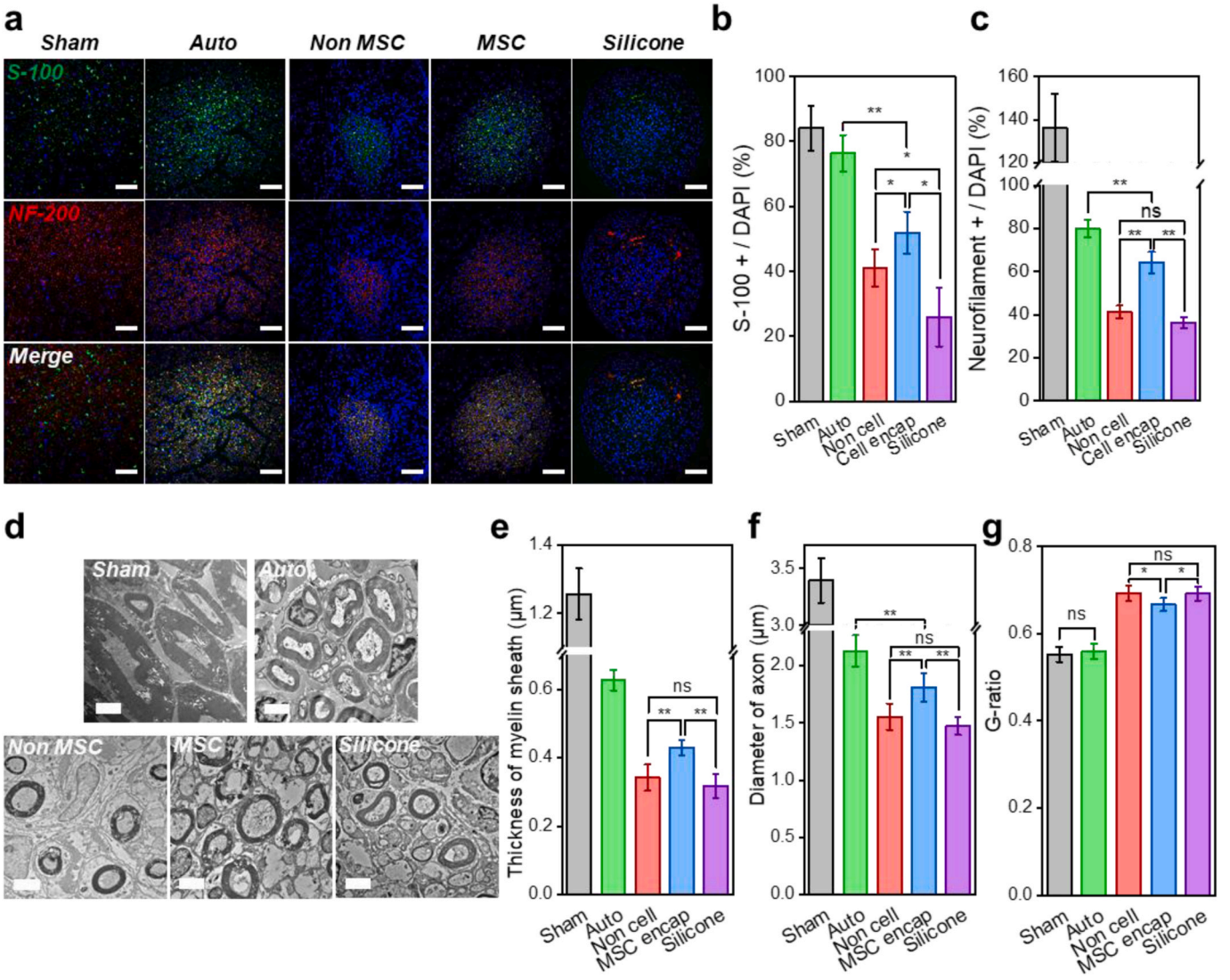

Fig. 6. Histological evaluation of the regenerated sciatic nerves. (a) Immunofluorescence images of the distal regions of regenerated sciatic nerves. S-100, NF-200, and nuclei (4′,6-diamidino-2-phenylindole [DAPI]) are indicated in green, red, and blue, respectively. Scale bars = 50 μm. (b) S-100 and (c) NF-200 staining areas normalized by DAPI staining areas in each sample (n = 5; *p < 0.05; **p < 0.01). (d) TEM images of the distal regions of regenerated nerves. Scale bars = 2 μm. (e) Thickness of myelin sheath (n = 5; **p < 0.01). (f) Diameter of axons (n = 5; **p < 0.01). (g) G-ratios of the regenerated nerves (n = 5; *p < 0.05).

arrays (Fig. 4j), suggesting that encapsulated ucMSCs induce vascularization in injured nerve tissues by secreting angiogenic molecules. Specifically, the MSCs incorporated within the DN hydrogels secreted high levels of pro-angiogenic factors such as HGF and GM-CSF (Fig. 4j), which promote endothelial cell migration and vessel formation. Furthermore, inflammatory response in vivo was analyzed by immunohistochemical staining for inducible nitric oxide synthase (iNOS), a marker for pro-inflammatory macrophages at 4 weeks post-implantation. The MSC-laden NGC group exhibited significantly reduced iNOS expression compared to control groups (Fig. S20), indicating attenuation of inflammatory reactions in nerve tissues. This anti-inflammatory effect appears to be mediated by the paracrine signaling of the encapsulated MSCs, which modulate immune responses and reduce M1 macrophage polarization, thereby creating a more favorable microenvironment for nerve regeneration.

Encapsulation of MSCs within DN hydrogel conduits offers several unique advantages over microsphere- or fiber-based delivery methods. Our strategy permits uniform cell distribution, supports sustained paracrine signaling, and maintains a permissive environment for Schwann cell migration and axonal elongation. In contrast, microspheres or fibers may hinder cell migration, limit factor diffusion or introduce fabrication complexity. Thus, MSC encapsulation within DN hydrogel NGCs provides a simple and effective approach for peripheral nerve repair.

Sciatic nerve injury leads to a reduction in the muscle fiber size, as described above. Muscle denervation inhibits muscle collagen degradation, resulting in the accumulation of fibrotic collagen in the muscle tissue [75]. Masson's trichrome staining of the gastrocnemius muscle at 12 weeks post-surgery revealed large muscle fibers with minimal scarring in the Sham, Auto, and MSC groups but irregular and small muscle fibers with significant scarring in the Non-MSC and Silicone groups (Fig. 7a). Specifically, MSC group (1027 ± 107 μm^2) exhibited a larger muscle fiber area than the Non-MSC (806 ± 143 μm^2) and Silicone (389 ± 64 μm^2) groups but a smaller muscle fiber area than the Sham (3396 ± 248 μm^2) and Auto groups (1395 ± 126 μm^2). In addition, fibrotic collagen deposition area of the MSC group (3.5 ± 0.7 %) was smaller

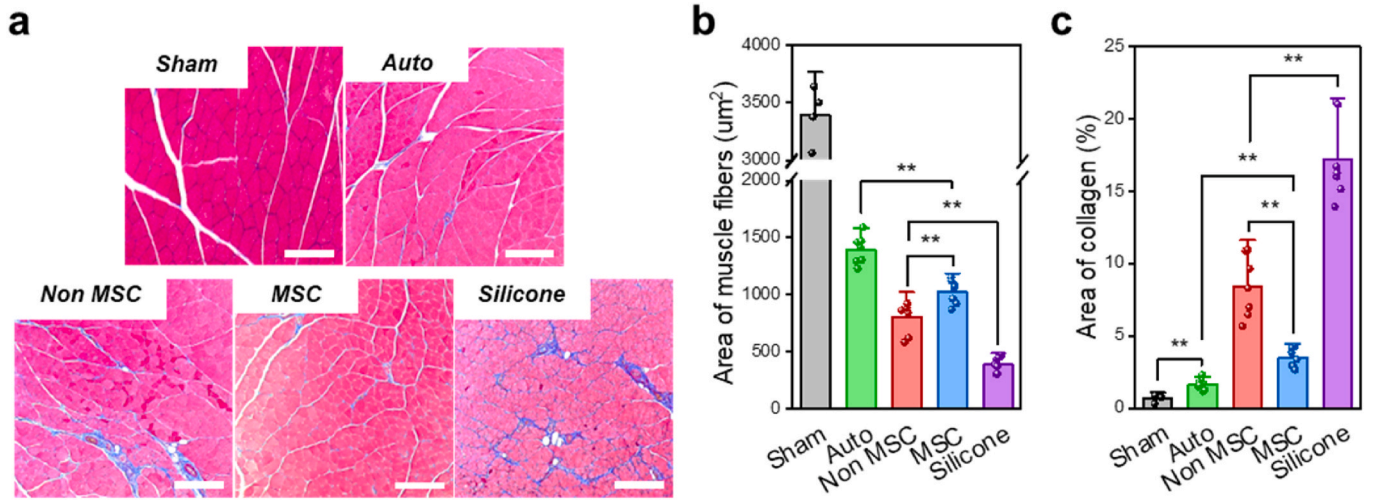

Fig. 7. Histological analysis of gastrocnemius muscles. Gastrocnemius muscles were analyzed 12 weeks after surgery and treatment. (a) Masson's trichrome staining images. Scale bars = 200 μm. Areas of (b) muscle fibers and (c) fibrotic collagen (n = 6; **p < 0.01).

area than those of the Non-MSC (8.4 ± 2.1 %) and Silicone (17.2 ± 2.8 %) groups but larger than that of the Sham (0.7 ± 0.3 %) and Auto groups (1.6 ± 0.4 %). Overall, our histochemical results suggest that ucMSC-laden NGCs effectively promote remyelination, axon regeneration, and muscle recovery.

4. Conclusion

To enhance peripheral nerve regeneration, we developed functional NGCs by encapsulating ucMSCs in DN hydrogels composed of GelMA and alginate. The established DN hydrogel NGCs exhibited excellent rheological and mechanical properties (e.g., fatigue resistance, suture retention, and kink resistance) for NGC applications. The encapsulated ucMSCs exerted potent neurogenic, angiogenic, and anti-inflammatory effects, as confirmed by various in vitro assays, including DRG, HUVEC, and RAW cell culture, secretome analyses, and in vivo studies using a 10-mm rat sciatic nerve defect model. Compared to the cell-free DN hydrogels and medical Silicone conduits, ucMSC-laden DN hydrogel NGCs significantly promoted nerve regeneration, as evidenced by improved axon maturation, remyelination, vascularization, and muscle recovery. Their efficacy was slightly lower but comparable to that of the gold standard autograft. Overall, our developed NGCs demonstrated excellent nerve regeneration performance. However, further optimization is necessary to achieve an efficacy comparable to or surpassing that of autografts using various cellular and material approaches (e.g., genetic engineering or potentiation of stem cells, incorporation of additional therapeutic substances, and engineering of stiffness and topography). We successfully demonstrated the regenerative efficacy of the MSC-laden DN hydrogel conduit in a rat sciatic nerve model. However, due to significant anatomical and physiological differences between rodent and human peripheral nerves, such as nerve size, fascicular complexity, and regeneration rates, further studies in large animal models are needed to confirm the safety, functionality, and scalability of this hydrogel conduit system for human application. Furthermore, DN hydrogel structure of NGCs has potential applications beyond peripheral nerve repair, serving as a promising platform for cell-based therapies in tissues such as the skin, tendons, muscles, and blood vessels. Collectively, our findings highlight the potential of NGCs for PNI treatment and other tissue engineering applications.

CRediT authorship contribution statement

Junghyun Kim: Writing – review & editing, Writing – original draft, Visualization, Methodology, Investigation. **Junggeon Park:** Methodology, Investigation. **Seungjun Lee:** Methodology, Investigation. **Chiseon Ryu:** Methodology, Investigation. **Jongdarm Yi:** Methodology, Investigation. **Goeun Choe:** Methodology. **Changhan Jo:** Methodology. **Jae Young Lee:** Writing – review & editing, Supervision, Resources, Funding acquisition, Conceptualization.

Data availability statement

Data supporting the findings of this study are available upon reasonable request from the corresponding author.

Ethics approval and consent to participate

All subjects gave their informed consent for inclusion before they participated in the study. All participants reviewed the methodological, ethical, legal and societal issues involved in the research and in the uses of animal study. All animal experiments were approved by the Animal Care and Use Committee of the Gwangju Institute of Science and Technology (approval number: GIST-2023-032). All experiments were approved by the local ethics committee of the Gwangju Institute of Science and Technology.

Declaration of competing interest

The authors declare that they have no known competing financial interests or personal relationships that could have appeared to influence the work reported in this paper.

Acknowledgements

This work was supported by a grant from the National Research Foundation of Korea (NRF) funded by the Ministry of Science, ICT, and Future Planning (RS-2023-NR076958 and RS-2021-NR057371).

Appendix A. Supplementary data

Supplementary data to this article can be found online at https://doi.org/10.1016/j.bioactmat.2025.08.018.

References

[1] J. Moskow, B. Ferrigno, N. Mistry, D. Jaiswal, K. Bulsara, S. Rudraiah, S. G. Kumbar, Review: bioengineering approach for the repair and regeneration of peripheral nerve, Bioact. Mater. 4 (2019) 107–113, https://doi.org/10.1016/j.bioactmat.2018.09.001.

[2] M.P. Lorei, E.B. Hershman, Peripheral nerve injuries in athletes, Sports Med. 16 (1993) 130–147, https://doi.org/10.2165/00007256-199316020-00005.
[3] J. Weng, P. Zhang, X. Yin, B. Jiang, The whole transcriptome involved in denervated muscle atrophy following peripheral nerve injury, Front. Mol. Neurosci. 11 (2018), https://doi.org/10.3389/fnmol.2018.00069.
[4] I. Ducic, J. Yoon, G. Buncke, Chronic postoperative complications and donor site morbidity after sural nerve autograft harvest or biopsy, Microsurgery 40 (2020) 710–716, https://doi.org/10.1002/micr.30588.
[5] W. Daly, L. Yao, D. Zeugolis, A. Windebank, A. Pandit, A biomaterials approach to peripheral nerve regeneration: bridging the peripheral nerve gap and enhancing functional recovery, J. R. Soc. Interface 9 (2011) 202–221, https://doi.org/10.1098/rsif.2011.0438.
[6] A. Zennifer, M. Thangadurai, D. Sundaramurthi, S. Sethuraman, Additive manufacturing of peripheral nerve conduits – fabrication methods, design considerations and clinical challenges, SLAS Technol. 28 (2023) 102–126, https://doi.org/10.1016/j.slast.2023.03.006.
[7] D. Arslantunali, T. Dursun, D. Yucel, N. Hasirci, V. Hasirci, Peripheral Nerve Conduits: Technology Update, Medical Devices: Evidence and Research, vol. 7, 2014, pp. 405–424, https://doi.org/10.2147/MDER.S59124.
[8] W.A. Lackington, A.J. Ryan, F.J. O'Brien, Advances in nerve guidance conduit-based therapeutics for peripheral nerve repair, ACS Biomater. Sci. Eng. 3 (2017) 1221–1235, https://doi.org/10.1021/acsbiomaterials.6b00500.
[9] J. Fang, L. Nan, K. Song, Z. Weng, J. Shan, V. Shahin, J. Liu, Y. Qian, Application and progress of bionic scaffolds in nerve repair: a narrative review, Advan. Technol. Neurosci. 1 (2024) 43, https://doi.org/10.4103/ATN.ATN-D-24-00004.
[10] J. Park, J. Jeon, B. Kim, M.S. Lee, S. Park, J. Lim, J. Yi, H. Lee, H.S. Yang, J.Y. Lee, Electrically conductive hydrogel nerve guidance conduits for peripheral nerve regeneration, Adv. Funct. Mater. 30 (2020) 2003759, https://doi.org/10.1002/adfm.202003759.
[11] E. Piantanida, G. Alonci, A. Bertucci, L. De Cola, Design of nanocomposite injectable hydrogels for minimally invasive surgery, Acc. Chem. Res. 52 (2019) 2101–2112, https://doi.org/10.1021/acs.accounts.9b00114.
[12] B.J. Parker, D.I. Rhodes, C.M. O'Brien, A.E. Rodda, N.R. Cameron, Nerve guidance conduit development for primary treatment of peripheral nerve transection injuries: a commercial perspective, Acta Biomater. 135 (2021) 64–86, https://doi.org/10.1016/j.actbio.2021.08.052.
[13] L. Thau, V. Reddy, P. Singh, Anatomy, central nervous system, in: StatPearls, StatPearls Publishing, Treasure Island (FL), 2024. http://www.ncbi.nlm.nih.gov/books/NBK542179/. (Accessed 26 July 2024).
[14] J.P. Gong, Why are double network hydrogels so tough? Soft Matter 6 (2010) 2583–2590, https://doi.org/10.1039/B924290B.
[15] Q. Chen, H. Chen, L. Zhu, J. Zheng, Engineering of tough double network hydrogels, Macromol. Chem. Phys. 217 (2016) 1022–1036, https://doi.org/10.1002/macp.201600038.
[16] J. Kim, J. Park, G. Choe, S.-I. Jeong, H.-S. Kim, J.Y. Lee, A gelatin/Alginate double network hydrogel nerve guidance conduit fabricated by a chemical-free gamma radiation for peripheral nerve regeneration, Adv. Healthcare Mater. 13 (2024) 2400142, https://doi.org/10.1002/adhm.202400142.
[17] Y. Wang, Z. Yan, W. Liu, C. Liu, N. Xu, Y. Wu, F. Sun, X. Wang, Y. Qian, L. Jiang, X. Sun, Biomechanically-adapted immunohydrogels reconstructing myelin sheath for peripheral nerve regeneration, Adv. Healthcare Mater. 11 (2022) 2201596, https://doi.org/10.1002/adhm.202201596.
[18] X. Yao, L. Zhan, Z. Yan, J. Li, L. Kong, X. Wang, H. Xiao, H. Jiang, C. Huang, Y. Ouyang, Y. Qian, C. Fan, Non-electric bioelectrical analog strategy by a biophysical-driven nano-micro spatial anisotropic scaffold for regulating stem cell niche and tissue regeneration in a neuronal therapy, Bioact. Mater. 20 (2023) 319–338, https://doi.org/10.1016/j.bioactmat.2022.05.034.
[19] A. Lavorato, S. Raimondo, M. Boido, L. Muratori, G. Durante, F. Cofano, F. Vincitorio, S. Petrone, P. Titolo, F. Tartara, A. Vercelli, D. Garbossa, Mesenchymal stem cell treatment perspectives in peripheral nerve regeneration: systematic review, Int. J. Mol. Sci. 22 (2021) 572, https://doi.org/10.3390/ijms22020572.
[20] M.J. Zargar, S. Kaviani, M. Vasei, M. Soufi Zomorrod, S. Heidari Keshel, M. Soleimani, Therapeutic role of mesenchymal stem cell-derived exosomes in respiratory disease, Stem Cell Res. Ther. 13 (2022) 194, https://doi.org/10.1186/s13287-022-02866-4.
[21] H.R. Hofer, R.S. Tuan, Secreted trophic factors of mesenchymal stem cells support neurovascular and musculoskeletal therapies, Stem Cell Res. Ther. 7 (2016) 131, https://doi.org/10.1186/s13287-016-0394-0.
[22] M. Kou, L. Huang, J. Yang, Z. Chiang, S. Chen, J. Liu, L. Guo, X. Zhang, X. Zhou, X. Xu, X. Yan, Y. Wang, J. Zhang, A. Xu, H. Tse, Q. Lian, Mesenchymal stem cell-derived extracellular vesicles for immunomodulation and regeneration: a next generation therapeutic tool? Cell Death Dis. 13 (2022) 1–16, https://doi.org/10.1038/s41419-022-05034-x.
[23] Y. Sowa, T. Imura, T. Numajiri, K. Nishino, S. Fushiki, Adipose-derived stem cells produce factors enhancing peripheral nerve regeneration: influence of age and anatomic site of origin, Stem Cell. Dev. 21 (2012) 1852–1862, https://doi.org/10.1089/scd.2011.0403.
[24] H. Zhou, Y. He, W. Xiong, S. Jing, X. Duan, Z. Huang, G.S. Nahal, Y. Peng, M. Li, Y. Zhu, Q. Ye, MSC based gene delivery methods and strategies improve the therapeutic efficacy of neurological diseases, Bioact. Mater. 23 (2023) 409–437, https://doi.org/10.1016/j.bioactmat.2022.11.007.
[25] M. Siemionow, M.M. Strojny, K. Kozlowska, S. Brodowska, W. Grau-Kazmierczak, J. Cwykiel, Application of human epineural conduit supported with human mesenchymal stem cells as a novel therapy for enhancement of nerve gap regeneration, Stem Cell Rev. Rep. 18 (2022) 642–659, https://doi.org/10.1007/s12015-021-10301-z.
[26] A.X. Sun, T.A. Prest, J.R. Fowler, R.M. Brick, K.M. Gloss, X. Li, M. DeHart, H. Shen, G. Yang, B.N. Brown, P.G. Alexander, R.S. Tuan, Conduits harnessing spatially controlled cell-secreted neurotrophic factors improve peripheral nerve regeneration, Biomaterials 203 (2019) 86–95, https://doi.org/10.1016/j.biomaterials.2019.01.038.
[27] X. Li, S. Chen, J. Li, X. Wang, J. Zhang, N. Kawazoe, G. Chen, 3D culture of chondrocytes in gelatin hydrogels with different stiffness, Polymers 8 (2016) 269, https://doi.org/10.3390/polym8080269.
[28] P. Tang, P. Song, Z. Peng, B. Zhang, X. Gui, Y. Wang, X. Liao, Z. Chen, Z. Zhang, Y. Fan, Z. Li, Y. Cen, C. Zhou, Chondrocyte-laden GelMA hydrogel combined with 3D printed PLA scaffolds for auricle regeneration, Mater. Sci. Eng. C 130 (2021) 112423, https://doi.org/10.1016/j.msec.2021.112423.
[29] K. Elkhoury, J. Zuazola, S. Vijayavenkataraman, Bioprinting the future using light: a review on photocrosslinking reactions, photoreactive groups, and photoinitiators, SLAS Technol. 28 (2023) 142–151, https://doi.org/10.1016/j.slast.2023.02.003.
[30] A. Sharir, M.M. Barak, R. Shahar, Whole bone mechanics and mechanical testing, Vet. J. 177 (2008) 8–17, https://doi.org/10.1016/j.tvjl.2007.09.012.
[31] A. Gonzalez-Pujana, A. Beloqui, J. Javier Aguirre, M. Igartua, E. Santos-Vizcaino, R. Maria Hernandez, Mesenchymal stromal cells encapsulated in licensing hydrogels exert delocalized systemic protection against ulcerative colitis via subcutaneous xenotransplantation, Eur. J. Pharm. Biopharm. 172 (2022) 31–40, https://doi.org/10.1016/j.ejpb.2022.01.007.
[32] M.T. Vurat, M. Parmaksiz, A.E. Elçin, Y.M. Elçin, Bioactive composite hydrogels as 3D mesenchymal stem cell encapsulation environment for bone tissue engineering: in vitro and in vivo studies, J. Biomed. Mater. Res. 111 (2023) 261–277, https://doi.org/10.1002/jbm.a.37457.
[33] C. Perner, C.L. Sokol, Protocol for dissection and culture of murine dorsal root ganglia neurons to study neuropeptide release, STAR Protocol. 2 (2021) 100333, https://doi.org/10.1016/j.xpro.2021.100333.
[34] A.R. Nectow, K.G. Marra, D.L. Kaplan, Biomaterials for the development of peripheral nerve guidance conduits, Tissue Eng. B Rev. 18 (2012) 40–50, https://doi.org/10.1089/ten.teb.2011.0240.
[35] F. Kanaya, J.C. Firrell, W.C. Breidenbach, Sciatic function index, nerve conduction tests, muscle contraction, and axon morphometry as indicators of regeneration, Plast. Reconstr. Surg. 98 (1996) 1264.
[36] F. Hug, K. Tucker, Surface electromyography to study muscle coordination, in: Handbook of Human Motion, Springer International Publishing, Cham, 2018, pp. 451–470, https://doi.org/10.1007/978-3-319-14418-4_184.
[37] Y. Kong, M. Kuss, Y. Shi, F. Fang, W. Xue, W. Shi, Y. Liu, C. Zhang, P. Zhong, B. Duan, Exercise facilitates regeneration after severe nerve transection and further modulates neural plasticity, Brain, Behav. Immun. - Health 26 (2022) 100556, https://doi.org/10.1016/j.bbih.2022.100556.
[38] Y. Zhang, X. Xu, Y. Tong, X. Zhou, J. Du, I.Y. Choi, S. Yue, G. Lee, B.N. Johnson, X. Jia, Therapeutic effects of peripherally administrated neural crest stem cells on pain and spinal cord changes after sciatic nerve transection, Stem Cell Res. Ther. 12 (2021) 180, https://doi.org/10.1186/s13287-021-02200-4.
[39] J.Y.F. Chang, H.P. Kessler, Masson trichrome stain helps differentiate myofibroma from smooth muscle lesions in the head and neck region, J. Formos. Med. Assoc. 107 (2008) 767–773, https://doi.org/10.1016/S0929-6646(08)60189-8.
[40] W. Pi, L. Zhou, W. Zhang, S. Liu, C. Li, M. Zhang, Y. Wen, P. Zhang, Three-dimensional conductive polycaprolactone/carbon nanotubes scaffolds for peripheral nerve regeneration, J. Mater. Sci. 57 (2022) 11289–11299, https://doi.org/10.1007/s10853-022-07336-z.
[41] W.-J. Chen, I.-H. Lin, C.-W. Lee, Y.-F. Chen, Aged skeletal muscle retains the ability to remodel extracellular matrix for degradation of collagen deposition after muscle injury, Int. J. Mol. Sci. 22 (2021) 2123, https://doi.org/10.3390/ijms22042123.
[42] T. Paus, R. Toro, Could sex differences in white matter be explained by g ratio? Front. Neuroanat. 3 (2009) https://doi.org/10.3389/neuro.05.014.2009.
[43] Ý.A. Mørch, I. Donati, B.L. Strand, G. Skjåk-Bræk, Effect of Ca2+, Ba2+, and Sr2+ on alginate microbeads, Biomacromolecules 7 (2006) 1471–1480, https://doi.org/10.1021/bm060010d.
[44] S. Saleki, S. Nouri Khorasani, S. Khalili, M. Hafezi, M. Najarzadegan, M. R. Molaviyan, M. Dinari, A. Kakapour, An injectable nanocomposite IPN hydrogel based on gelatin Methacrylate/Alginate/COF for tissue engineering applications, Macromol. Mater. Eng. 309 (2024) 2300417, https://doi.org/10.1002/mame.202300417.
[45] E. Jamshidifar, M. Esfandyari-Manesh, H. Motasadizadeh, S. Naderizadeh, A. Yourdkhani, N. Samadi, R. Dinarvand, Improvement of in vitro osteogenesis and anti-infection properties by GelMA scaffold containing levofloxacin nanoparticles and strontium microspheres for osteomyelitis, J. Mater. Sci. 57 (2022) 13603–13619, https://doi.org/10.1007/s10853-022-07456-6.
[46] D.F.S. Fonseca, P.C. Costa, I.F. Almeida, P. Dias-Pereira, I. Correia-Sá, V. Bastos, H. Oliveira, C. Vilela, A.J.D. Silvestre, C.S.R. Freire, Swellable gelatin methacryloyl microneedles for extraction of interstitial skin fluid toward minimally invasive monitoring of urea, Macromol. Biosci. 20 (2020) 2000195, https://doi.org/10.1002/mabi.202000195.
[47] K. Rahali, G. Ben Messaoud, C.J.F. Kahn, L. Sanchez-Gonzalez, M. Kaci, F. Cleymand, S. Fleutot, M. Linder, S. Desobry, E. Arab-Tehrany, Synthesis and characterization of nanofunctionalized gelatin methacrylate hydrogels, Int. J. Mol. Sci. 18 (2017) 2675, https://doi.org/10.3390/ijms18122675.
[48] Q. Chen, X. Tian, J. Fan, H. Tong, Q. Ao, X. Wang, An interpenetrating alginate/gelatin network for three-dimensional (3D) cell cultures and organ bioprinting, Molecules 25 (2020) 756, https://doi.org/10.3390/molecules25030756.

[49] R. Birch, R. Birch, R. Birch, R. Birch, The peripheral nervous system: anatomy and function, in: R. Birch (Ed.), Peripheral Nerve Injuries: a Clinical Guide, Springer, London, 2013, pp. 1–67, https://doi.org/10.1007/978-1-4471-4613-1_1.
[50] B.A. Clements, J. Bushman, N.S. Murthy, M. Ezra, C.M. Pastore, J. Kohn, Design of barrier coatings on kink-resistant peripheral nerve conduits, J. Tissue Eng. 7 (2016) 2041731416629471, https://doi.org/10.1177/2041731416629471.
[51] D. Shahriari, M. Shibayama, D.A. Lynam, K.J. Wolf, G. Kubota, J.Y. Koffler, M. H. Tuszynski, W.M. Campana, J.S. Sakamoto, Peripheral nerve growth within a hydrogel microchannel scaffold supported by a kink-resistant conduit, J. Biomed. Mater. Res. 105 (2017) 3392–3399, https://doi.org/10.1002/jbm.a.36186.
[52] A. Escobar, A. Serafin, M.R. Carvalho, M. Culebras, A. Cantarero, A. Beaucamp, R. L. Reis, J.M. Oliveira, M.N. Collins, Electroconductive poly(3,4-ethylenedioxythiophene) (PEDOT) nanoparticle-loaded silk fibroin biocomposite conduits for peripheral nerve regeneration, Adv. Compos. Hybrid Mater. 6 (2023) 118, https://doi.org/10.1007/s42114-023-00689-2.
[53] Q. Quan, H. Meng, B. Chang, L. Hong, R. Li, G. Liu, X. Cheng, H. Tang, P. Liu, Y. Sun, J. Peng, Q. Zhao, Y. Wang, S. Lu, Novel 3-D helix-flexible nerve guide conduits repair nerve defects, Biomaterials 207 (2019) 49–60, https://doi.org/10.1016/j.biomaterials.2019.03.040.
[54] A. Wilkins, K. Kemp, M. Ginty, K. Hares, E. Mallam, N. Scolding, Human bone marrow-derived mesenchymal stem cells secrete brain-derived neurotrophic factor which promotes neuronal survival *in vitro*, Stem Cell Res. 3 (2009) 63–70, https://doi.org/10.1016/j.scr.2009.02.006.
[55] P. Carmeliet, Blood vessels and nerves: common signals, pathways and diseases, Nat. Rev. Genet. 4 (2003) 710–720, https://doi.org/10.1038/nrg1158.
[56] P. Wu, Z. Tong, L. Luo, Y. Zhao, F. Chen, Y. Li, C. Huselstein, Q. Ye, Q. Ye, Y. Chen, Comprehensive strategy of conduit guidance combined with VEGF producing Schwann cells accelerates peripheral nerve repair, Bioact. Mater. 6 (2021) 3515–3527, https://doi.org/10.1016/j.bioactmat.2021.03.020.
[57] H.M. Kwon, S.-M. Hur, K.-Y. Park, C.-K. Kim, Y.-M. Kim, H.-S. Kim, H.-C. Shin, M.-H. Won, K.-S. Ha, Y.-G. Kwon, D.H. Lee, Y.-M. Kim, Multiple paracrine factors secreted by mesenchymal stem cells contribute to angiogenesis, Vasc. Pharmacol. 63 (2014) 19–28, https://doi.org/10.1016/j.vph.2014.06.004.
[58] W. Dai, Y. Yang, Y. Yang, W. Liu, Material advancement in tissue-engineered nerve conduit, Nanotechnol. Rev. 10 (2021) 488–503, https://doi.org/10.1515/ntrev-2021-0028.
[59] P. Hernández-Cortés, J. Garrido, M. Cámara, F.O. Ravassa, Failed digital nerve reconstruction by foreign body reaction to Neurolac® nerve conduit, Microsurgery 30 (2010) 414–416, https://doi.org/10.1002/micr.20730.
[60] C. Wang, H. Koh, S. Ramakrishna, S. Liao, 9 - nerve tissue regeneration, in: L. A. Bosworth, S. Downes (Eds.), Electrospinning for Tissue Regeneration, Woodhead Publishing, 2011, pp. 168–201, https://doi.org/10.1533/9780857092915.2.168.
[61] H. Yang, Q. Li, L. Li, S. Chen, Y. Zhao, Y. Hu, L. wang, X. Lan, L. Zhong, D. Lu, Gastrodin modified polyurethane conduit promotes nerve repair via optimizing Schwann cells function, Bioact. Mater. 8 (2022) 355–367, https://doi.org/10.1016/j.bioactmat.2021.06.020.
[62] X. Dong, S. Liu, Y. Yang, S. Gao, W. Li, J. Cao, Y. Wan, Z. Huang, G. Fan, Q. Chen, H. Wang, M. Zhu, D. Kong, Aligned microfiber-induced macrophage polarization to guide schwann-cell-enabled peripheral nerve regeneration, Biomaterials 272 (2021) 120767, https://doi.org/10.1016/j.biomaterials.2021.120767.
[63] A.L. Bombeiro, B.T.N. Pereira, A.L.R. de Oliveira, Granulocyte-macrophage colony-stimulating factor improves mouse peripheral nerve regeneration following sciatic nerve crush, Eur. J. Neurosci. 48 (2018) 2152–2164, https://doi.org/10.1111/ejn.14106.
[64] N. Lee, S.H. Lee, J. Lee, M.-Y. Lee, J. Lim, S. Kim, S. Kim, Hepatocyte growth factor is necessary for efficient outgrowth of injured peripheral axons in *in vitro* culture system and *in vivo* nerve crush mouse model, Biochem. Biophys. Rep. 26 (2021) 100973, https://doi.org/10.1016/j.bbrep.2021.100973.
[65] K.R. Ko, J. Lee, D. Lee, B. Nho, S. Kim, Hepatocyte Growth Factor (HGF) promotes peripheral nerve regeneration by activating repair schwann cells, Sci. Rep. 8 (2018) 8316, https://doi.org/10.1038/s41598-018-26704-x.
[66] B.E. Fornasari, G. Carta, G. Gambarotta, S. Raimondo, Natural-based biomaterials for peripheral nerve injury repair, Front. Bioeng. Biotechnol. 8 (2020), https://doi.org/10.3389/fbioe.2020.554257.
[67] A. Muheremu, Q. Ao, Past, present, and future of nerve conduits in the treatment of peripheral nerve injury, BioMed Res. Int. 2015 (2015) 237507, https://doi.org/10.1155/2015/237507.
[68] C.R. Carvalho, J.M. Oliveira, R.L. Reis, Modern trends for peripheral nerve repair and regeneration: beyond the hollow nerve guidance conduit, Front. Bioeng. Biotechnol. 7 (2019), https://doi.org/10.3389/fbioe.2019.00337.
[69] X. Tang, X. Gu, T. Huang, X. Chen, Z. Zhou, Y. Yang, J. Ling, Anisotropic silk-inspired nerve conduit with peptides improved the microenvironment for long-distance peripheral nerve regeneration, ACS Macro Lett. 10 (2021) 1501–1509, https://doi.org/10.1021/acsmacrolett.1c00533.
[70] G. Duan, C. Li, X. Yan, S. Yang, S. Wang, X. Sun, L. Zhao, T. Song, Y. Pan, X. Wang, Construction of a mineralized collagen nerve conduit for peripheral nerve injury repair, Regen. Biomater. 10 (2023) rbac089, https://doi.org/10.1093/rb/rbac089.
[71] J. Park, J. Kim, G. Choe, Y. Jung, J.Y. Lee, Conductive hydrogel luminal filler for peripheral nerve regeneration, Biomaterials 317 (2025) 123103, https://doi.org/10.1016/j.biomaterials.2025.123103.
[72] X. Mao, T. Li, J. Cheng, M. Tao, Z. Li, Y. Ma, R. Javed, J. Bao, F. Liang, W. Guo, X. Tian, J. Fan, T. Yu, Q. Ao, Nerve ECM and PLA-PCL based electrospun bilayer nerve conduit for nerve regeneration, Front. Bioeng. Biotechnol. 11 (2023), https://doi.org/10.3389/fbioe.2023.1103435.
[73] M. Fernandes, S.G. Valente, R.G. Sabongi, J.B. Gomes dos Santos, V.M. Leite, H. Ulrich, A.A. Nery, M.J. da Silva Fernandes, Bone marrow-derived mesenchymal stem cells versus adipose-derived mesenchymal stem cells for peripheral nerve regeneration, Neural Regenerat. Res. 13 (2018) 100, https://doi.org/10.4103/1673-5374.224378.
[74] M. El Soury, Ó.D. García-García, I. Tarulli, J. Chato-Astrain, I. Perroteau, S. Geuna, S. Raimondo, G. Gambarotta, V. Carriel, Chitosan conduits enriched with fibrin-collagen hydrogel with or without adipose-derived mesenchymal stem cells for the repair of 15-mm-long sciatic nerve defect, Neural Regenerat. Res. 18 (2023) 1378, https://doi.org/10.4103/1673-5374.358605.
[75] A. Yadav, R. Dabur, Skeletal muscle atrophy after sciatic nerve damage: mechanistic insights, Eur. J. Pharmacol. 970 (2024) 176506, https://doi.org/10.1016/j.ejphar.2024.176506.
[76] K.R. Jessen, R. Mirsky, The repair Schwann cell and its function in regenerating nerves, J. Physiol. 594 (2016) 3521–3531, https://doi.org/10.1113/JP270874.
[77] H. Xu, Y. Yan, S. Li, PDLLA/chondroitin sulfate/chitosan/NGF conduits for peripheral nerve regeneration, Biomaterials 32 (2011) 4506–4516, https://doi.org/10.1016/j.biomaterials.2011.02.023.
[78] S.N. Lawson, P.J. Waddell, Soma neurofilament immunoreactivity is related to cell size and fibre conduction velocity in rat primary sensory neurons, J. Physiol. 435 (1991) 41–63, https://doi.org/10.1113/jphysiol.1991.sp018497.
[79] H. Wang, M. Wu, C. Zhan, E. Ma, M. Yang, X. Yang, Y. Li, Neurofilament proteins in axonal regeneration and neurodegenerative diseases, Neural Regen Res 7 (2012) 620–626, https://doi.org/10.3969/j.issn.1673-5374.2012.08.010.
[80] Å.F. Svennigsen, L.B. Dahlin, Repair of the peripheral Nerve—Remyelination that works, Brain Sci. 3 (2013) 1182–1197, https://doi.org/10.3390/brainsci3031182.
[81] T. Chomiak, B. Hu, What is the optimal value of the g-Ratio for myelinated fibers in the rat CNS? A theoretical approach, PLoS One 4 (2009) e7754, https://doi.org/10.1371/journal.pone.0007754.
[82] P. Yang, Y. Peng, X. Dai, J. Jie, D. Kong, X. Gu, Y. Yang, Bionic peptide scaffold in situ polarization and recruitment of M2 macrophages to promote peripheral nerve regeneration, Bioact. Mater. 30 (2023) 85–97, https://doi.org/10.1016/j.bioactmat.2023.07.003.